COLLEGE OF ENGINEERING

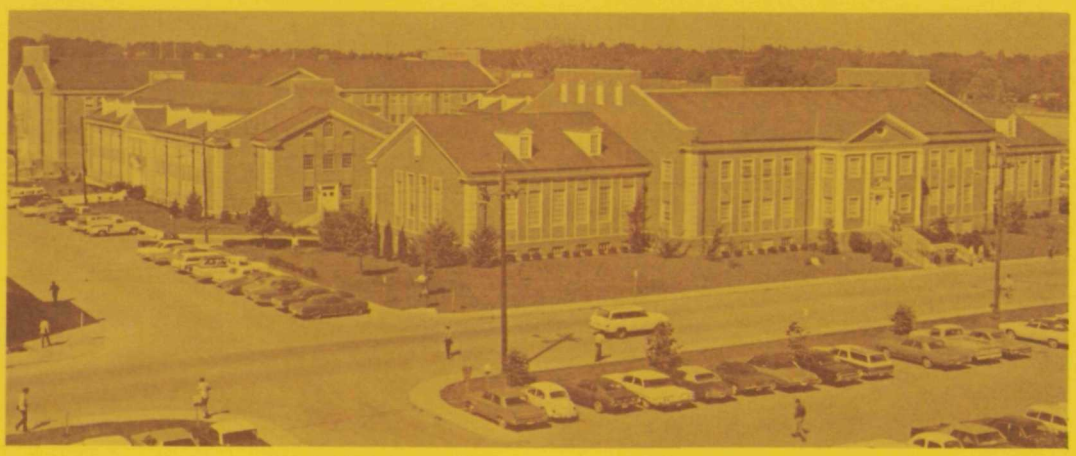

Engineering Complex

TENNESSEE TECHNOLOGICAL UNIVERSITY
COOKEVILLE, TENNESSEE

AN INVESTIGATION OF THE OPEN-LOOP AMPLIFICATION OF REYNOLDS NUMBER DEPENDENT PROCESSES BY WAVE DISTORTION -- ANNUAL REPORT

by

Kenneth R. Purdy, Marie B. Ventrice

and

Jih-Chin Fang

TENNESSEE TECHNOLOGICAL UNIVERSITY

December 1972

prepared for

NATIONAL AERONAUTICS AND SPACE ADMINISTRATION

Lewis Research Center

Grant NGR 43-003-015

R. J. Priem, Technical Monitor

FOREWORD

This report was prepared by the staff of Tennessee Technological University, Cookeville, Tennessee on Grant NGR 43-003-015 for Lewis Research Center, National Aeronautics and Space Administration. The research was administered under the technical cognizance of Dr. Richard J. Priem, Head of the Rocket Combustion Section. Dr. Priem's interest in the work is deeply appreciated.

ABSTRACT

Analytical and experimental studies were initiated to determine if the response of a constant temperature hot wire anemometer to acoustic oscillations could serve as an analog to the response of the drop vaporization burning rate process to acoustic oscillations, and, perhaps, also as an analog to any Reynolds number dependent process. The motivation behind this study was a recent analytical study which showed that distorted acoustic oscillations could amplify the open-loop response of vaporization limited combustion. This type of amplification may be the cause of unstable combustion in liquid propellant rocket engines.

The analytical results obtained to date for the constant temperature anemometer are similar in nature to those previously obtained for vaporization limited combustion and indicate that the response is dependent on the amount and type of distortion as well as other factors, such as sound pressure level, Mach number and hot wire temperature.

In the experimental portion of the work, a system was designed and built which can create the same type of environment for the hot wire as was used in the theoretical analysis and which can determine the response for those conditions. Preliminary results indicate qualitative agreement between theory and experiment.

TABLE OF CONTENTS

LIST OF FIGURES

Figure Page

NOMENCLATURE

Sybmol	
A_w	hot wire surface area
A, B	hot wire constants
$\tilde{A}$, $\tilde{B}$, $\tilde{C}$	functions defined by (18)
c_∞	speed of sound at T_∞
D	diameter of test section
D_w	hot wire diameter
E	hot wire bridge voltage
$\tilde{E}$	total energy
h	heat transfer coefficient
I	hot wire current
I_{nl}	nonlinear out-of-phase response factor
K	hot wire sensitivity to flow parallel to its axis
k	thermal conductivity of air
L	length of test section
L_w	hot wire length
Nu	Nusselt number (hD_w/k_f)
n	harmonic order (n = 1,2,3,...)
P	air pressure
P_∞	undisturbed air pressure
P'_{rms}	rms pressure amplitude $\left[\frac{1}{2}\sum_{n=1}^{\infty} p_n^2\right]^{0.5}$
p_n	harmonic pressure perturbation coefficient
R	normalized cross correlation coefficient
R_a	gas constant for air
R_{cbl}	cable resistance

Symbol

Re	Reynolds number ($\rho_g VD_w/\mu_f$)
R_o	hot wire resistance at T_o
R_p	probe resistance
R_s	standard resistance
R_w	hot wire resistance at T_w
R_∞	hot wire resistance at T_∞
R_{nl}	nonlinear in-phase response factor
Q	heat transfer
T	air temperature
T_f	film temperature, $1/2[T_w + T_\infty]$
T_∞	undisturbed air temperature
T_n	harmonic temperature perturbation coefficient
T_o	reference temperature
T_w	hot wire temperature
t	time
u,v,w,	cartesian components of velocity (x,y,z)
V	wire cooling velocity
v_θ, v_r, v_z	cylindrical components of velocity (θ,r,z)
v_n	harmonic transverse air velocity coefficient
v_t	transverse air velocity
W	work transfer
x,y,z	cartesian coordinates
θ,r,z,	cylindrical coordinates

Greek Symbols

α	hot wire resistance coefficient
$\hat{\alpha}$	hot wire angle of inclination to radius vector
α_{10}	eigen value (0.5861)

Greek Symbols

γ	ratio of specific heats
θ_n	harmonic phase angle for velocity-pressure relation
ρ	air density
ρ_n	harmonic density perturbation coefficient
ϕ_n	harmonic phase angle for pressure perturbation
μ	air absolute viscosity
ω	radian frequency

Superscripts

'	time-dependent component
-	time-mean component
~	dimensionless property

Subscripts

f	evaluation at film temperature
o	value at $T = T_o = 0°C$
∞	undisturbed value

Chapter 1

INTRODUCTION

Setting

The need exists to obtain a more accurate understanding of the nonlinear instability limits of rocket engines. These limits are currently one of the least understood properties of combustion instability. The causes of instability and the factors determining the instability limits are of major importance to the design of high performance rocket engines.

Steady combustion in liquid propellant rockets is assumed to be vaporization limited. Priem and Heidmann [1] have shown that quantitative agreement exists between theory and experiment. Vaporization limited combustion is also expected for unstable combustion and this has been qualitatively confirmed.

Recently, Heidmann [2,3] has shown analytically that distorted acoustic oscillations affect the open-loop response of vaporization limited combustion--a velocity sensitive, or Reynolds number dependent, process. In particular, the open-loop response factor increased as the level of distortion increased. Response factors an order of magnitude greater than that obtained for sinusoidal excitation were found for some conditions.

The vaporization model used in references 2 and 3 assumed that the burning rate was proportional to the drop Reynolds number raised

to a power. Such a model characterizes Reynolds number dependent processes other than drop vaporization burning rates. Thus, the results of references 2 and 3, and of this research, may also be of significance to convective heat and mass transfer processes in general.

Intent

The objective of this research is to experimentally confirm the results of Heidmann's studies by determining the open-loop response of a Reynolds number dependent process which is an analog of the drop-vaporization burning-rate process. An analogous process, which lends itself to direct measurement of the flow quantities, will greatly simplify the work over that of attempting to make measurements in a burning mixture. The ultimate objective, towards which this research is directed, is to determine the closed-loop response of the drop varpoization process to distorted acoustic waves; i.e., to determine if rocket combustion will become unstable when excited by distorted waves.

The work to confirm Heidmann's results can be categorized as follows:

- Engineering analysis of the open-loop response of the analog process to distorted waves. This is necessary to meaningfully interpret the experimental results.
- Design and construction of a test system to measure the in-phase open-loop response factor for the analog process.
- Measurement of the open-loop response factor for spinning transverse acoustic oscillations generated by pure sinusoidal and distorted sinusoidal input signals. This mode of oscillation

would be studied since it is the most frequently encountered mode in unstable combustion [3]. Variations in the through-flow velocity, the harmonic amplitudes and the harmonic phase angles would be considered.

- Comparison of the measured response factors with those predicted.

At this time the first two items have been largely completed. The last two items are still in the preliminary stage. Each item will be separately discussed.

Chapter 2

ANALYTICAL STUDY

The Analog

A qualitative description of the drop vaporization process will provide a basis for choosing a suitable analog. First we have a liquid droplet at a temperature close to its saturation temperature corresponding to the partial pressure of its vapor. The gas mixture, which surrounds the droplet, moves relative to it and has a temperature which is often significantly larger than the droplet's. Much of the energy transfer from the gas mixture to the droplet is by forced convection and, under steady-state conditions, results in vaporization of the droplet liquid.

Assuming the drop vaporization process to be convection dominated, a reasonable analog of this process is that of forced convection heat transfer from a hot wire to a cool gas. Since the constant-temperature hot-wire anemometer provides an excellent means for experimentally determining the instantaneous energy transfer rate from a hot wire, it is being used as the analog process.

To provide a controlled unsteady environment for the hot wire, a resonant sound field with forced mean gas motion will be used. Before giving a detailed description of the wire's environment, the physics of a constant-temperature hot wire in an unsteady gas flow will be developed.

Hot-Wire Physics

Physical System

The physical system is shown in figure 1. It is assumed there exists a steady mean flow, U, and that the wire is oriented such that its axis is normal to the mean flow direction. For the cartesian coordinate system shown in figure 1, the x-axis is in the mean flow direction and the z-axis is parallel to the cylinder's axis.

Energy is electrically supplied to the wire such that its temperature is constant -- the constant-temperature anemometer provides the needed energy and controls. A natural limitation for the anemometer, however, is that the gas temperature must not exceed the normal operating temperature of the wire.

Energy Analysis

Taking the hot wire to be a closed system, the first law of thermodynamics is

$$\frac{dQ}{dt} - \frac{dW}{dt} = \frac{d\tilde{E}}{dt} . \tag{1}$$

For constant temperature operation the total energy of the wire is constant and (1) becomes

$$\frac{dQ}{dt} = \frac{dW}{dt} . \tag{2}$$

The rate of electrical work done by the system is

$$\frac{dW}{dt} = - I^2 R_w . \tag{3}$$

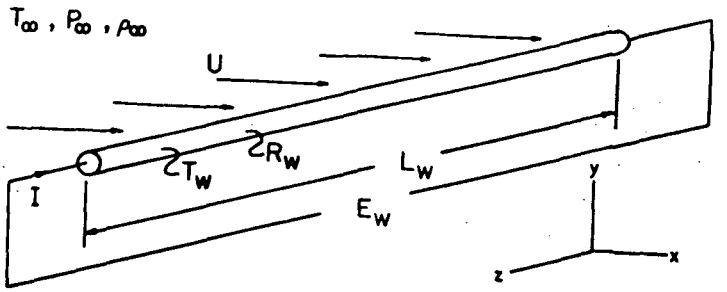

Figure 1. Schematic Diagram of the Hot Wire and Its Environment.

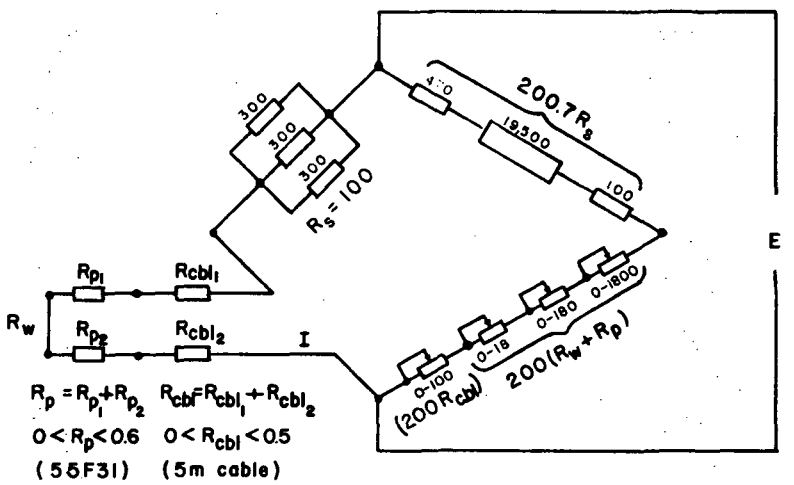

Figure 2. Disa Hot-Wire Bridge Network.

Three modes of energy transfer as heat exist. However, radiation is small enough to be neglected, conduction and convection are lumped together, and Newton's law of cooling is used to express the heat transfer rate; that is,

$$\frac{dQ}{dt} = - hA_w[T_w - T_\infty]. \tag{4}$$

Introducing the Nusselt number,

$$Nu_f = \frac{hD_w}{k_f}, \tag{5}$$

equations (2), (3) and (4) reduce to

$$I^2R_w = \pi k_f L_w Nu_f[T_w - T_\infty] . \tag{6}$$

Auxiliary Relations

Certain auxiliary relations are now introduced to permit (6) to be expressed in terms of the properties normally measured and/or known.

The electrical resistance of the wire is practically a linear function of temperature. Expressed mathematically, this is

$$R_w = R_o + \alpha[T_w - T_o], \tag{7}$$

where R_o is the wire resistance at T_o -- $T_o = 0°C$ in this analysis. Letting R_∞ denote the wire resistance when it is in thermal equilibrium with its environment, the wire over-temperature is

$$T_w - T_\infty = \frac{R_w - R_\infty}{\alpha} . \tag{8}$$

In the DISA anemometer system, the potential drop across the wire is not directly measured, and it is necessary to express the current in

(6) in terms of the DISA bridge properties. For the bridge network shown in figure 2 (on page 6), the hot-wire current is

$$I = \frac{E}{R_s + R_{cbl} + R_p + R_w} . \tag{9}$$

There are a number of possible correlations that could be used to express Nu_f in terms of the flow field variables. One of the most reliable correlation forms, for low Reynolds number flows ($0.02<Re_f<44$), seems to be that of the Collis-Williams equation [4], namely

$$Nu_f = [A + B\ Re_f^{0.45}][T_f/T_\infty]^{0.17}, \tag{10}$$

where: A, B — dimensionless constants (A is a strong function of wire length when $L_w/D_w < 400$ and B seems to be a weak function of L_w/D_w.),

Re_f — wire Reynolds number, $\rho_f\ V\ D_w/\mu_f$,

V — wire cooling velocity, $[(\bar{u} + u')^2 + (v')^2 + K(w')^2]^{0.5}$,

$()_f$ — property evaluated at the film temperature, and

T_f — film temperature, $1/2\ [T_w + T_\infty]$.

Since the experiments will use atmospheric air at room temperature and pressure, the viscosity and thermal conductivity data will be taken from Hilsenrath [5] and the density will be computed from the ideal gas relation, namely,

$$\rho = \frac{P}{R_a T} \tag{11}$$

with

$$R_a = 287.06\ \frac{m^2}{sec^2\text{-}^\circ K} .$$

The Hilsenrath data in the temperature range of interest ($273.15°K < T < 473.15°K$), can be accurately approximated by

$$k = k_o[T/T_o]^{0.877}, \tag{12}$$

and

$$\mu = \mu_o[T/T_o]^{0.757}, \tag{13}$$

with

$$k_o = 2.413 \times 10^{-2} \frac{kg\text{-}m}{sec\ \text{-}K^\circ},$$

$$\mu_o = 1.716 \times 10^{-5} \frac{kg}{sec\text{-}m}, \text{ and}$$

$$T_o = 273.15°K.$$

Bridge Voltage - Flow Property Relationship

The relationship between the hot-wire bridge voltage and the flow properties is obtained by combining (6), (7), (9), (10), (11), (12) and (13). This gives

$$E^2 = \left[\frac{[R_s + R_{cbl} + R_p + R_w]^2}{R_w}\right][\pi L_w k_o][A + B\ Re_{f_o}{}^{0.45}(\tilde{V}^2)^{0.225}]\cdot$$

$$\left[\frac{T_f}{T_\infty}\right]^{0.17}\left[\frac{T_f}{T_o}\right]^{0.877}[T_w - T_\infty], \tag{14}$$

where

$$R_w = R_o + \alpha[T_w - T_o], \tag{7}$$

$$T_f = 0.5\ [T_w + T_\infty], \tag{15}$$

$$Re_{f_o} = \frac{P_\infty V_o D_w}{R_a T_f \mu_o [T_f/T_o]^{0.757}} \tag{16}$$

$$V_o = 1 \frac{m}{sec},$$

$$\tilde{V}^2 = [(\bar{u} + u')^2 + (v')^2 + K(w')^2]/V_o^2, \text{ and} \tag{17}$$

$$K = 0.$$

It was assumed that the wire is not cooled by fluid motion parallel to its axis and thus K was set equal to zero.

Since the empirical relationship for Nu_f, equation (10), was obtained for steady-state, steady-flow conditions, its applicability to unsteady flow is questionable. However, it is customary to assume that it holds for unsteady flows if instantaneous values are substituted for the fluid properties. This is done here and it constitutes a major assumption.

Noting that the leading coefficient in (14) is constant during normal operation, and that it depends on the wire temperature, (14) can be rewritten in a simpler form by defining dimensional forms of A and B, namely,

$$\tilde{A} = \tilde{C}(T_w)A, \tag{18a}$$

$$\tilde{B} = \tilde{C}(T_w)B, \tag{18b}$$

where

$$\tilde{C}(T_w) = \pi L_w k_o \left[\frac{[R_s + R_{cbl} + R_p + R_w]^2}{R_w}\right]. \tag{18c}$$

With this nomenclature the final form of (14) becomes

$$E = \left[[\tilde{A} + \tilde{B}\ Re_f^{0.45}(\tilde{V}^2)^{0.225}] \left[\frac{T_f}{T_\infty}\right]^{0.17} \left[\frac{T_f}{T_o}\right]^{0.877} [T_w - T_\infty] \right]^{0.5}. \quad (19)$$

To determine E, the flow field properties must be known.

Flow Field Properties

The flow field providing the wire's environment is schematically shown in figure 3. The cylindrical enclosure, with inside diameter D and length L, is acoustically closed but permits a uniform forced flow in the axial direction.

With proper excitation of this enclosure, acoustic velocity oscillations in any of the three vector directions can be obtained. However, Heidmann [3] restricted his analysis to transverse-velocity oscillations -- "because of the greater interest in transverse-mode instability in rocket combustors." Considering only transverse oscillations, the hot-wire cooling velocity can be expressed as

$$V^2 = \bar{u}^2 + (v')^2. \quad (20)$$

Noting that V^2 is given in terms of velocity components based on the wire's cartesian coordinate system, it is necessary to relate these velocity components to those based on the enclosure's cylindrical system. The wire is oriented (figure 3) such that its axis is in the r-θ plane and makes the angle $\hat{\alpha}$ with the radius vector. Thus

$$\bar{u} = \bar{v}_z, \quad (21)$$

$$v' = v_r \sin \hat{\alpha} + v_\theta \cos \hat{\alpha}, \quad (22)$$

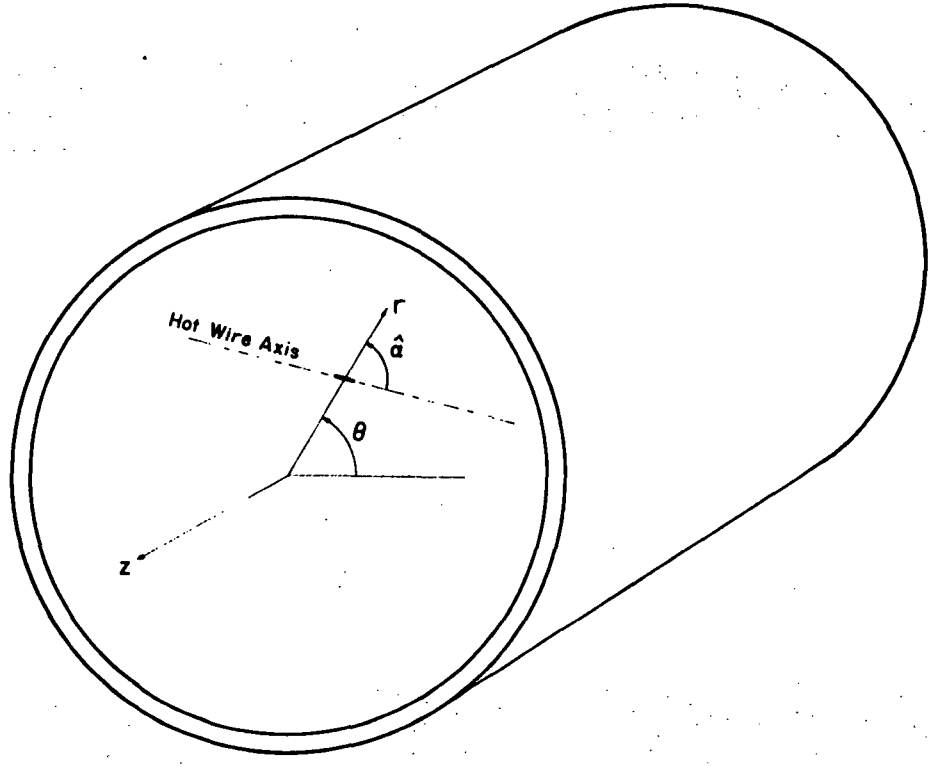

Figure 3. Schematic Diagram of the Hot Wire In Its Cylindrical Enclosure.

and (20) becomes

$$V^2 = \bar{v}_z^2 \left[1 + \tilde{v}_r \sin \hat{\alpha} + \tilde{v}_\theta \cos \hat{\alpha})^2\right], \tag{23}$$

with

$$\tilde{v}_r = v_r/\bar{v}_z,$$

and

$$\tilde{v}_\theta = v_\theta/\bar{v}_z.$$

All the other properties that are affected by the acoustic oscillations, thereby having acoustic components, will be expressed in the form

$$\beta = \bar{\beta} + \beta' \tag{24}$$

or

$$\beta = \bar{\beta}\left[1 + \tilde{\beta}'\right], \tag{25}$$

where $\bar{\beta}$ is the time-mean component of the general property β, β' is its acoustic component, and $\tilde{\beta}'$ is its "normalized" acoustic component -- $\tilde{\beta}' = \beta'/\bar{\beta}$.

The expressions used for the normalized acoustic components are the same as those in reference 3, namely

$$\tilde{P}' = \sum_{n=1}^{\infty} p_n \cos(n\omega t - \phi_n),$$

$$\tilde{\rho}' = \sum_{n=1}^{\infty} \rho_n \cos(n\omega t - \phi_n),$$

$$\tilde{T}' = \sum_{n=1}^{\infty} T_n \cos(n\omega t - \phi_n),$$

$$\tilde{v}_t = \sum_{n=1}^{\infty} v_n \cos(n\omega t - \phi_n - \theta_n),$$

$$v_t = v_r,$$

and

$$\tilde{v}_t = v_t/\bar{v}_z. \tag{26}$$

The expression for $\tilde{T}'$ has been added to those given by Heidmann. The phase angle ϕ_n specifies the phase relation between harmonic components. It has been assumed to be identical for acoustic pressure, density and temperature. The gas velocity expression also contains ϕ_n but it is further modified by a velocity phase angle θ_n which specifies the velocity-pressure phase relations. When θ_n is zero, the velocity and pressure are in phase and traveling wave properties are simulated. A θ_n of 90° simulates standing acoustic modes.

Nonlinear Response Factor

Exposing a constant-temperature hot wire to a mean flow perturbed by acoustic oscillations results in an unsteady hot-wire energy transfer which is exhibited as an unsteady hot-wire voltage E. Expressed in terms of its mean and fluctuating components, E is

$$E = \bar{E} + E', \tag{27}$$

or

$$E = \bar{E}\,[1 + \tilde{E}'], \tag{28}$$

with

$$\tilde{E}' = E'/\bar{E}. \tag{29}$$

A parameter which compares that portion of $\tilde{E}'$ which is in phase

with the acoustic pressure $\tilde{P}'$ is the nonlinear in-phase response factor defined by

$$R_{n\ell} = \frac{\int_0^{2\pi} \tilde{E}'(\omega t)\, \tilde{P}'(\omega t)\, d(\omega t)}{\int_0^{2\pi} [\tilde{P}'(\omega t)]^2\, d(\omega t)} . \tag{30}$$

A parameter which compares that portion of $\tilde{E}'$ which is in phase with the 90-degree-phase-shifted acoustic pressure $\tilde{P}'_{ps}$ is the nonlinear out-of-phase response factor defined by

$$I_{n\ell} = \frac{\int_0^{2\pi} \tilde{E}'(\omega t)\, \tilde{P}'_{ps}(\omega t)\, d(\omega t)}{\int_0^{2\pi} [\tilde{P}'_{ps}(\omega t)]^2\, d(\omega t)} , \tag{31}$$

where

$$\tilde{P}'_{ps}(\omega t) = \sum_{n=1}^{\infty} p_n \cos(n\omega t - \phi_n - \pi/2),$$

or

$$\tilde{P}'_{ps}(\omega t) = \sum_{n=1}^{\infty} p_n \sin(n\omega t - \phi_n). \tag{32}$$

Equations (30) and (31) are based on the approximation given by

$$\tilde{E}'(\omega t) = R_{n\ell}\, \tilde{P}'(\omega t) + I_{n\ell}\, \tilde{P}'_{ps}(\omega t). \tag{33}$$

To evaluate $R_{n\ell}$ and $I_{n\ell}$, $\tilde{E}'(\omega t)$ must be related to the sound field given by equations (26). This is done in the following manner:

• The hot wire's properties, including its operating temperature, are specified.

• The hot wire's environment is specified. This includes the time-mean through-flow velocity $\bar{v}_z$, the time-mean absolute temperature and pressure of the air, and the sound field.

• The instantaneous value of each property is concomitantly substituted in (19), thereby producing $E(\omega t)$.

• The time-mean value of $E(\omega t)$, $\bar{E}$, is obtained from

$$\bar{E} = \frac{1}{2\pi} \int_0^{2\pi} E(\omega t)\, d(\omega t). \tag{34}$$

Due to the complex mathematical form of $E(\omega t)$, the integration is normally performed numerically.

• The desired $\tilde{E}'(\omega t)$ is given by

$$\tilde{E}'(\omega t) = [E(\omega t) - \bar{E}]/\bar{E}. \tag{35}$$

With $\tilde{E}'(\omega t)$ given by (35) and $\tilde{P}'(\omega t)$ given by (26), $R_{n\ell}$ and $I_{n\ell}$ are obtained from (30) and (31), respectively. The nature of the nonlinear response factors is best illustrated by numerical examples.

Numerical Examples

The numerical examples to be presented are based on the following hot-wire and environmental properties:

• Wire and Bridge Properties

$L_w = 1.02$ mm

$D_w = 5$ μm

$$\alpha = 0.0129 \text{ ohm/K}^\circ$$

$$R_p = 0.40 \text{ ohm}$$

$$R_{cbl} = 0.30 \text{ ohm}$$

$$R_s = 100 \text{ ohm}$$

$$R_w = [0.0129\ T_w(^\circ K) - 0.08] \text{ ohm}$$

- Basic Air Properties

$$T_o = 273.15^\circ K$$

$$k_o = 2.413 \times 10^{-2} \text{ kg-m/(sec}^3\text{-K}^\circ\text{)}$$

$$\mu_o = 1.716 \times 10^{-5} \text{ kg/(sec-m)}$$

$$R_a = 287.06 \text{ m}^2\text{/(sec-K}^\circ\text{)}$$

$$\gamma = 1.4$$

$$V_o = 1 \text{ m/sec}$$

- Wire Environmental Properties

$$T_\infty = \bar{T} = 295.37^\circ K$$

$$P_\infty = P = 738.9 \text{ mm Hg}$$

$$L = 30.48 \text{ cm}$$

$$D = 20.42 \text{ cm}$$

With these properties specified, the main variables are: the hot-wire Mach number $M = \bar{v}_z/c_\infty$, the hot-wire temperature T_w, and the acoustic properties.

Traveling Acoustic Waves

The examples for traveling waves will be for the first traveling transverse mode of resonance with the wire oriented such that $\theta = 0$ and $\hat{\alpha} = 0$ (the wire's axis is parallel to the radius vector). For radial positions outside the acoustic boundary layer region, the acoustic density, temperature and particle velocity are simply related to the

acoustic pressure, assuming the harmonic components of the acoustic properties are related to those of the acoustic pressure in the same manner that they are for undistorted waves. With this assumption the harmonic components of equations (26) are related to the p_n in the following manner:

$$\rho_n = \frac{1}{\gamma} p_n,$$

$$T_n = \frac{\gamma-1}{\gamma} p_n,$$

$$v_n = -\frac{1}{\gamma} \frac{R/r}{\pi\alpha_{10}} p_n,$$

and

$$\theta_n = 0. \tag{36}$$

Heidmann's [3] velocity coefficient differs with that of (36) by its sign and the radially dependent coefficient $R/(\pi\alpha_{10}r)$. The sign difference has no effect on the response factor. For purposes of comparison, the radial position will be taken as that for which $R = \pi\alpha_{10}r$. Thus the harmonic velocity components are given by

$$v_n = -\frac{1}{\gamma} p_n. \tag{37}$$

Influence of Harmonic Content on $R_{n\ell}$. Considering sound pressure wave distortion due only to the second harmonic of p_1 (i.e., due to p_2), the nonlinear in-phase response factor was computed. The results are displayed graphically in figure 4 for various ratios of p_2 to p_1. For this Mach number ($M = 0.005$), maximum response seems to occur for a normalized root-mean-square sound pressure level of 0.00692 and for p_2/p_1

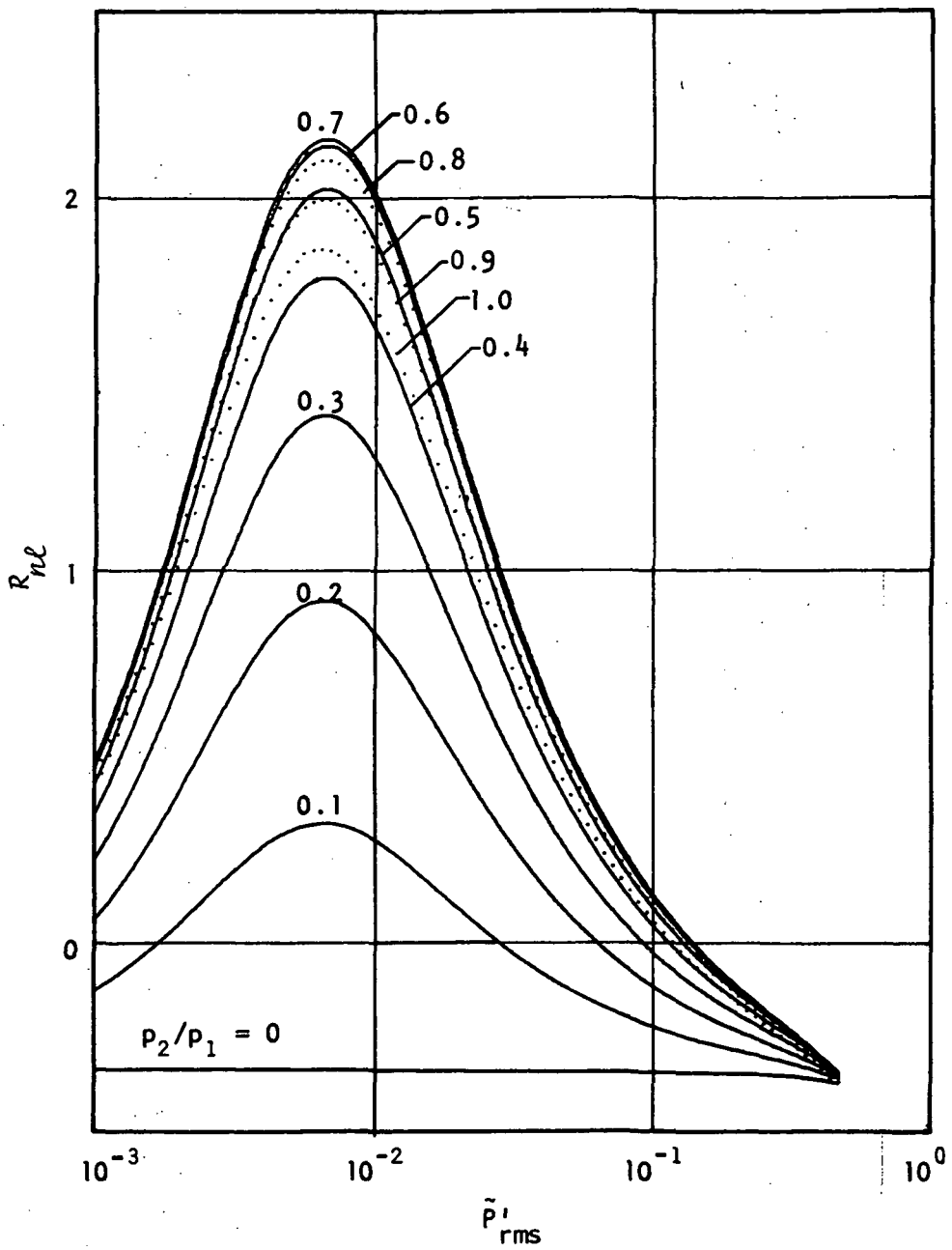

Figure 4. Nonlinear In-Phase Response Factor Versus Root-Mean-Square Sound Pressure Level for Various Harmonic Contents; $M = 0.005$, $\phi_1 = \phi_2 = \theta_1 = \theta_2 = 0$, $T_w - T_\infty = 100\ K°$.

approximately equal to 0.7. Figure 4 is similar in form to Heidmann's [3] figure 2c. Note, however, that peak response occurs at a lower value of $\tilde{P}'_{rms}$ for the hot-wire.

The value of p_2/p_1 for which $R_{n\ell}$ is a maximum (0.7) is clearly demonstrated in figure 5. From the three curves presented it is seen that this value is not dependent on the sound pressure level.

Influence of Mach Number on $R_{n\ell}$. For a fixed pressure waveform ($p_2/p_1 = 0.7$), $R_{n\ell}$ was computed for various wire Mach numbers. The results are shown in figure 6. Generally speaking, the lower the Mach number, the greater the response. This is more clearly shown in figure 7, where three different harmonic contents are considered.

It should be noted, in figure 6, that the value of the sound level at which peak response occurs increases with increasing Mach number.

Comparing Heidmann's [3] figure 7 with figure 6 it is seen that they agree in form.

Influence of Wire Overtemperature on $R_{n\ell}$. The influence of wire overtemperature on the peak response for the conditions of figure 4 is now considered. Fixing the sound field conditions ($p_2/p_1 = 0.7$, $\tilde{P}'_{rms} = 0.00692$), the effect of wire overtemperature on $R_{n\ell}$ is shown in figure 8. Note that $R_{n\ell}$ reaches its maximum value at about $T_w - T_\infty = 175$ K°.

Influence of Harmonic Phase Angle on $I_{n\ell}$ and $R_{n\ell}$. The influence of ϕ_2 on the nonlinear response factors for the conditions of peak $R_{n\ell}$ of figure 4, except for ϕ_2, is shown in figure 9. Note that $I_{n\ell}$

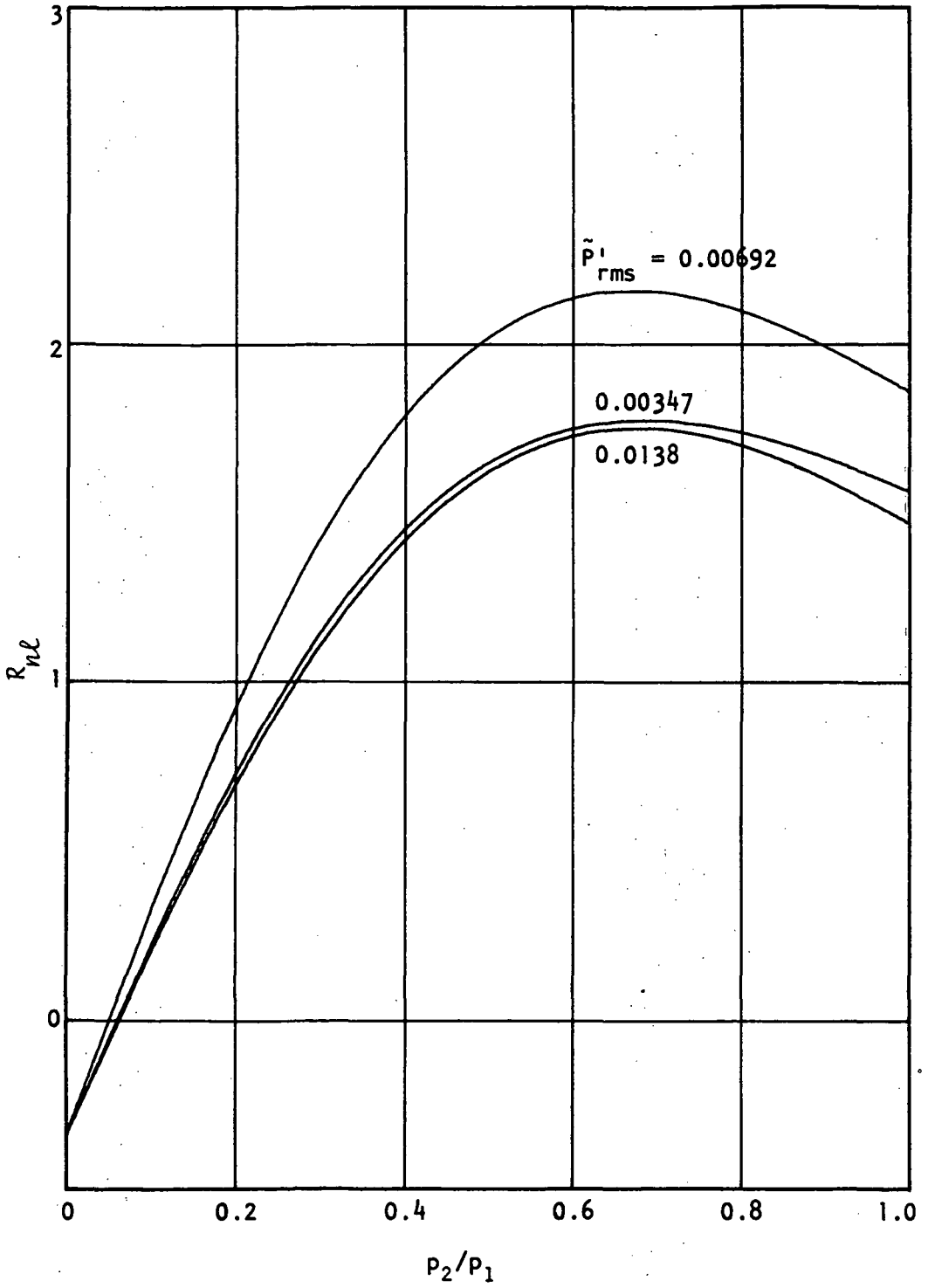

Figure 5. Nonlinear In-Phase Response Factor Versus Harmonic Content for Various Sound Pressure Levels; M = 0.005, $\phi_1 = \phi_2 = \theta_1 = \theta_2 = 0$, $T_w - T_\infty = 100$ K°.

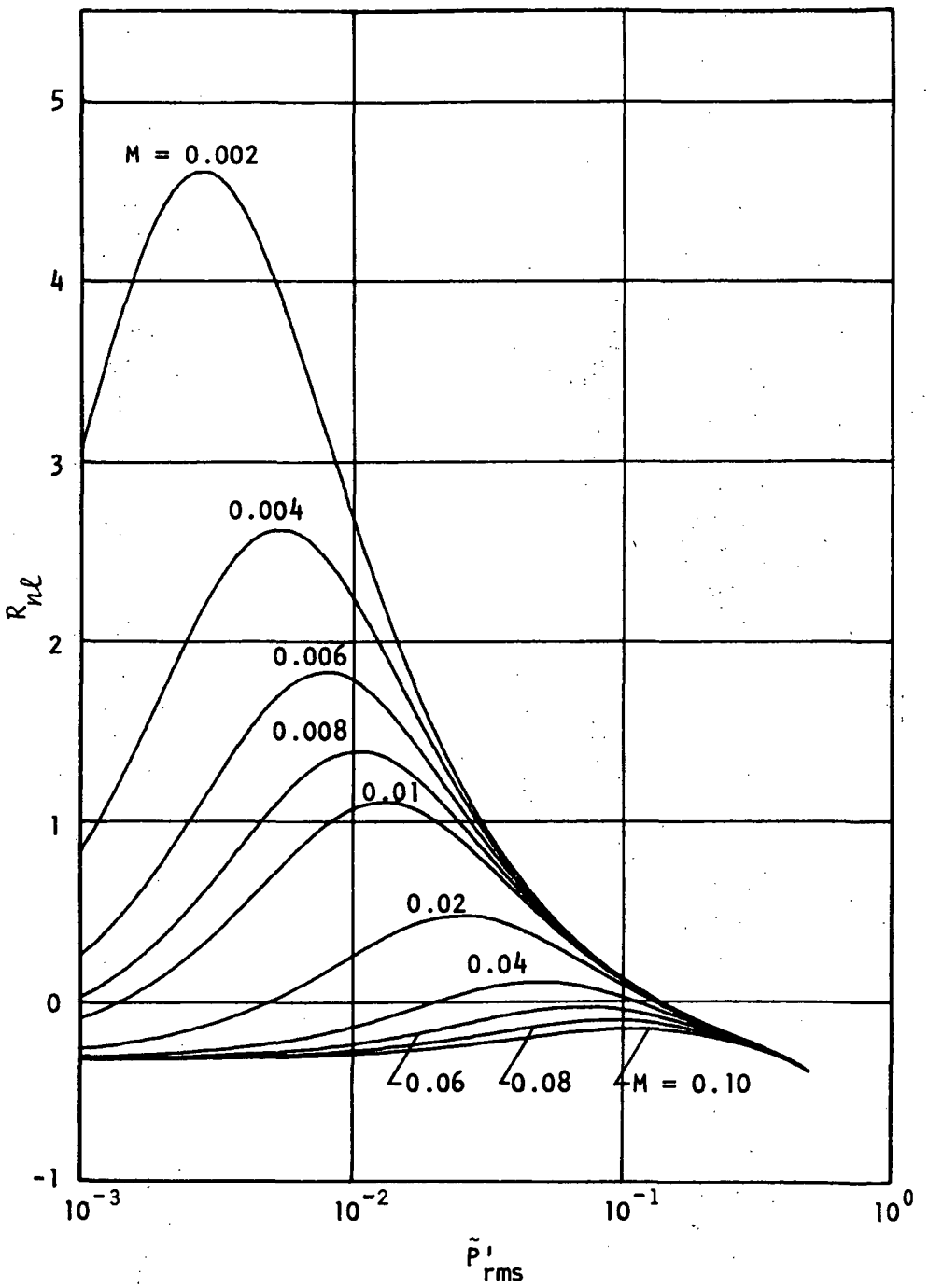

Figure 6. Nonlinear In-Phase Response Factor Versus Root-Mean-Square Sound Pressure Level for Various Mach Numbers; $\phi_1 = \phi_2 = \theta_1 = \theta_2 = 0$, $T_w - T_\infty = 100$ K°, $p_2/p_1 = 0.7$.

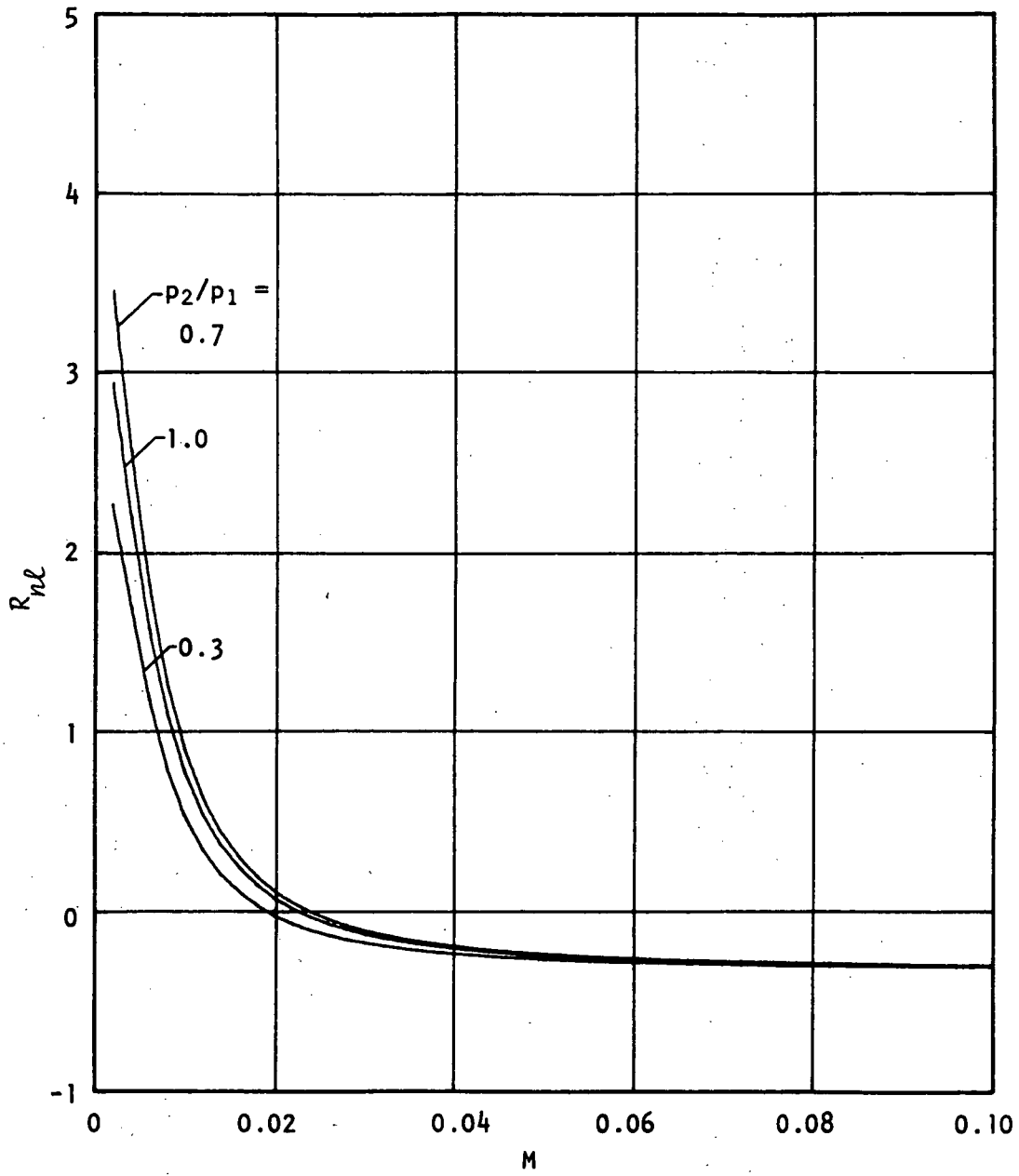

Figure 7. Nonlinear In-Phase Response Factor Versus Mach Number for Various Harmonic Contents; $\phi_1 = \phi_2 = \theta_1 = \theta_2 = 0$, $T_w - T_\infty = 100$ K°, $\tilde{P}'_{rms} = 0.00692$.

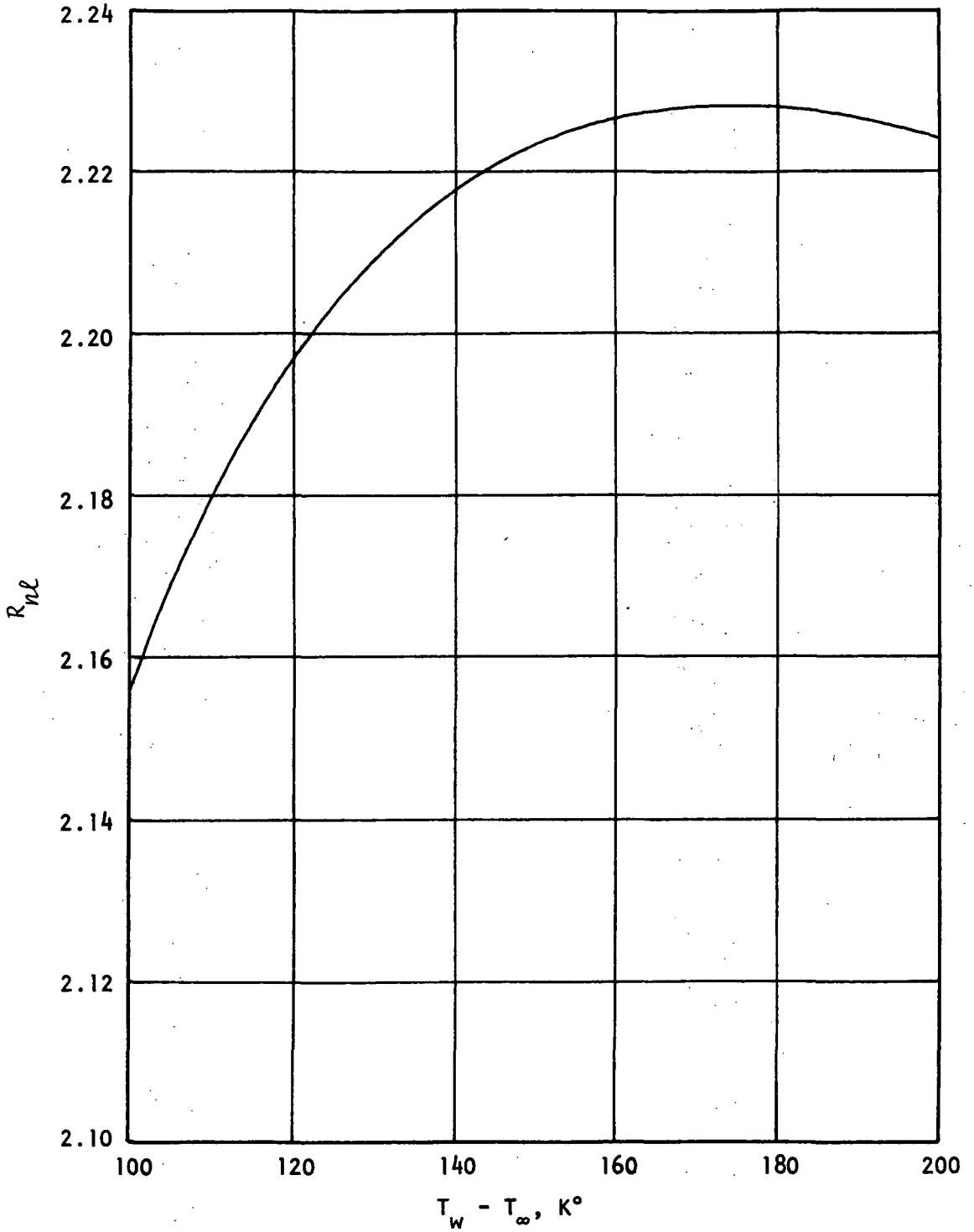

Figure 8. Nonlinear In-Phase Response Factor Versus Hot Wire Overtemperature; $M = 0.005$, $\phi_1 = \phi_2 = \theta_1 = \theta_2 = 0$, $p_2/p_1 = 0.7$, $\tilde{P}'_{rms} = 0.00692$.

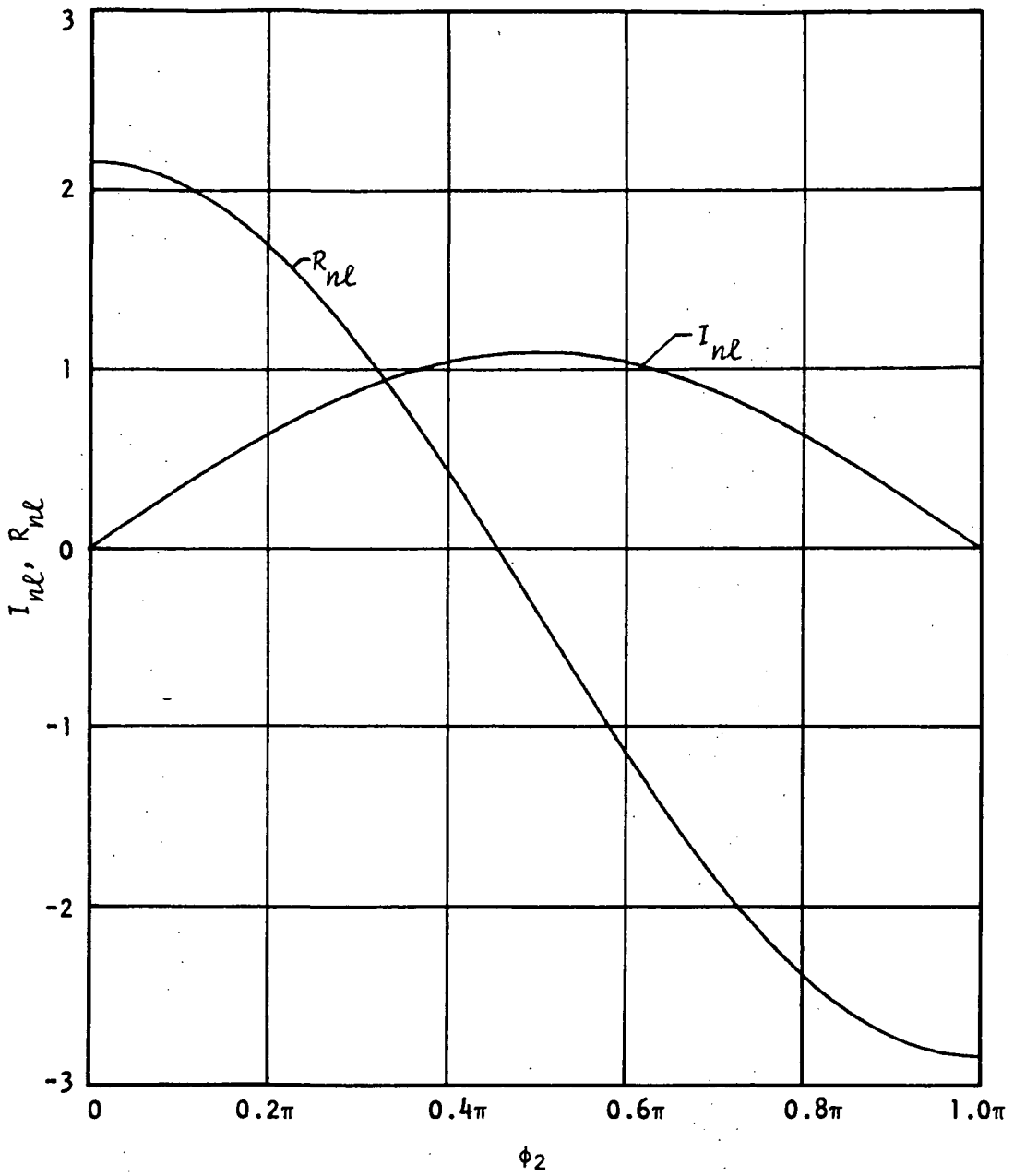

Figure 9. Nonlinear Response Factors Versus Phase Angle Between Fundamental Sound Pressure Component and Its Second Harmonic; $M = 0.005$, $\phi_1 = \theta_1 = \theta_2 = 0$, $p_2/p_1 = 0.7$, $\tilde{P}'_{rms} = 0.00692$, $T_w - T_\infty = 100$ K°.

is zero for ϕ_2 = 0 and 180 degrees and that it takes on its maximum positive value at ϕ_2 = 90 degrees. The in-phase response factor has its maximum at ϕ_2 = 0 degrees.

Figure 9 is similar to Heidmann's [3] figure 6. It is a cut of his figure at peak response.

Influence of Velocity Phase Angle on $I_{n\ell}$ and $R_{n\ell}$. By again using the sound field properties that produced the peak value of $R_{n\ell}$ in figure 4, the effect of θ on the nonlinear response factors was determined and the results are shown in figure 10.

The in-phase factor $R_{n\ell}$ in this figure represents a cross-correlogram of $\tilde{E}'$ and $\tilde{P}'$ and the out-of-phase factor $I_{n\ell}$ is a cross-correlogram of $\tilde{E}'$ and $\tilde{P}'_{ps}$. Both of these can be obtained experimentally.

Figure 10 represents a cut of Heidmann's figure 5 at peak response.

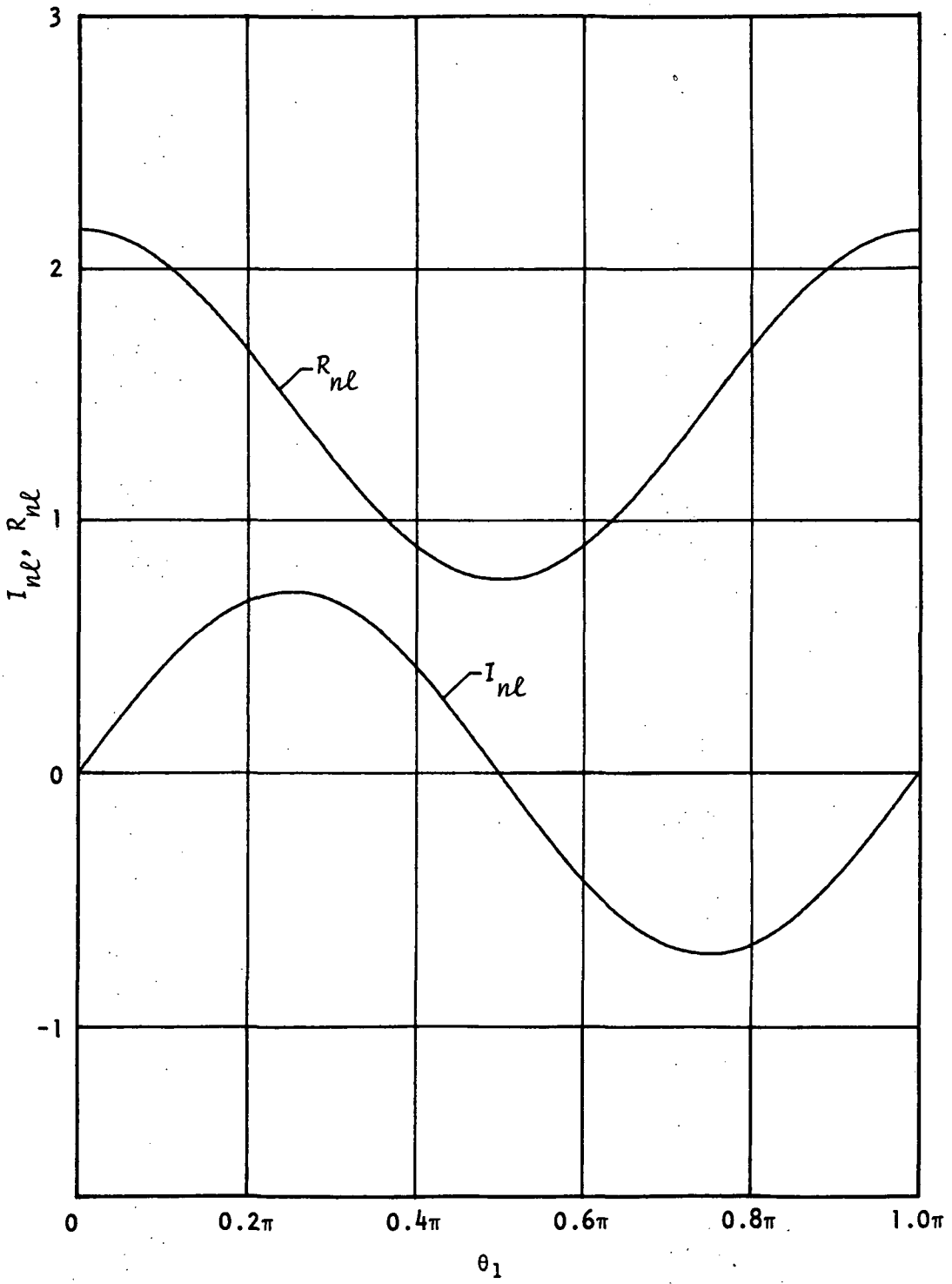

Figure 10. Nonlinear Response Factors Versus Velocity Phase Angle; $M = 0.005$, $\phi_1 = \phi_2 = 0$, $\theta_2 = \theta_1$, $T_w - T_\infty = 100\ K°$, $p_2/p_1 = 0.7$, $P'_{rms} = 0.00692$.

Chapter 3

EXPERIMENTAL STUDY

The object of the experimental portion of the research is to determine the open loop response of a constant temperature hot-wire anemometer to distorted acoustic oscillations, and to compare the results with those obtained theoretically. An experimental system is needed which will create the same velocity and acoustic environment as that used in the analytical portion of the work. It is also desirable to incorporate maximum flexibility into the system so that it can be readily adapted to any future work.

The system needed consists of four basic parts -- the test section itself, a means of generating the necessary acoustic oscillations, a means of analyzing the data, and the various types of equipment needed to monitor the performance of all parts of the system. Figure 11 is a schematic illustration of the system and figures 12 and 13 show two different views of the completed system.

Apparatus

Test Section

The test section is an aluminum cylinder with a 20.42 cm I.D., 25.4 cm O.D., and an effective inside length of 30.48 cm. The ends of the cylinder are closed with 1.27 cm thick circular aluminum plates into which approximately 310 equally spaced 2.54 mm diameter holes have been

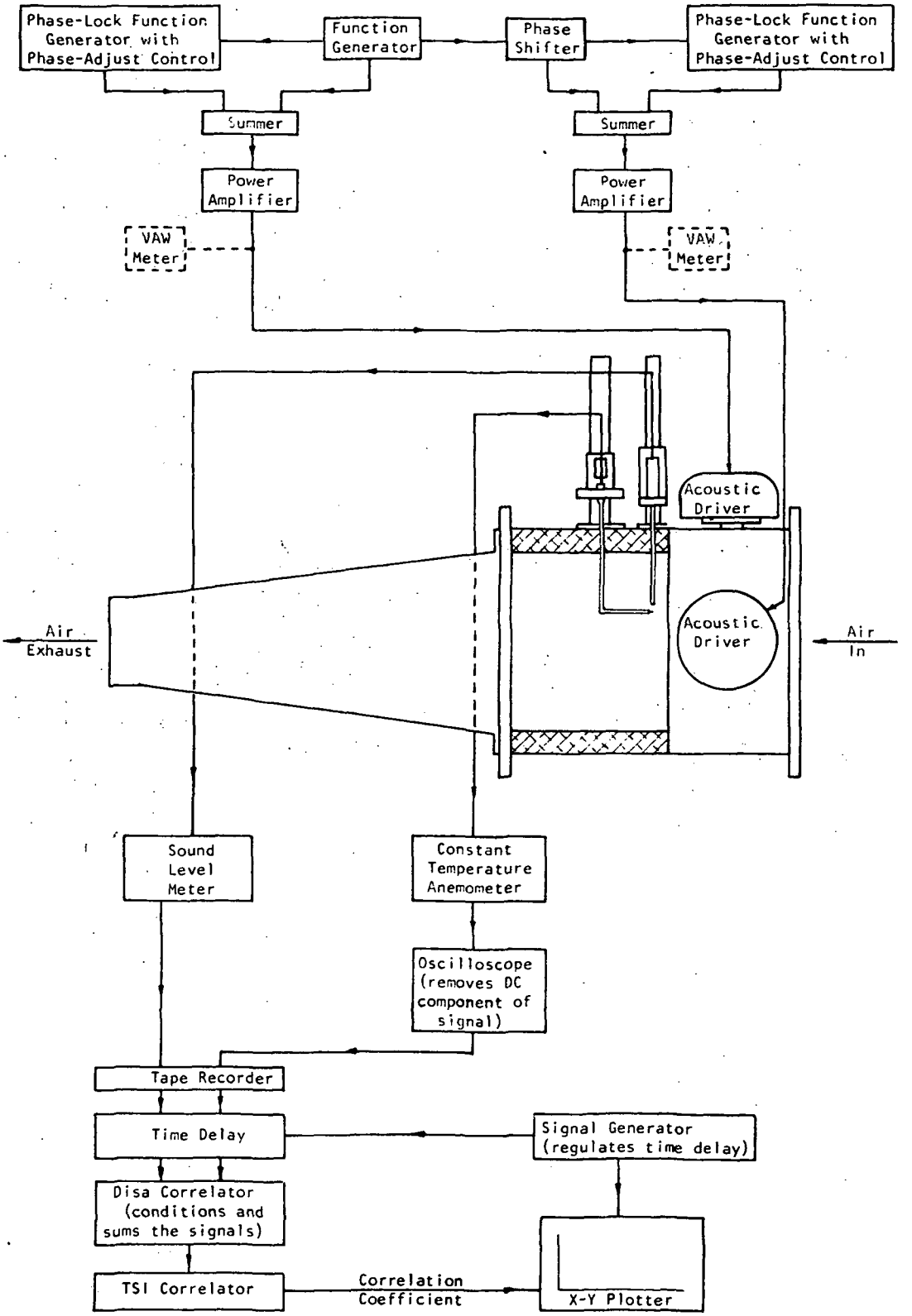

Figure 11. Schematic Diagram of the Experimental System.

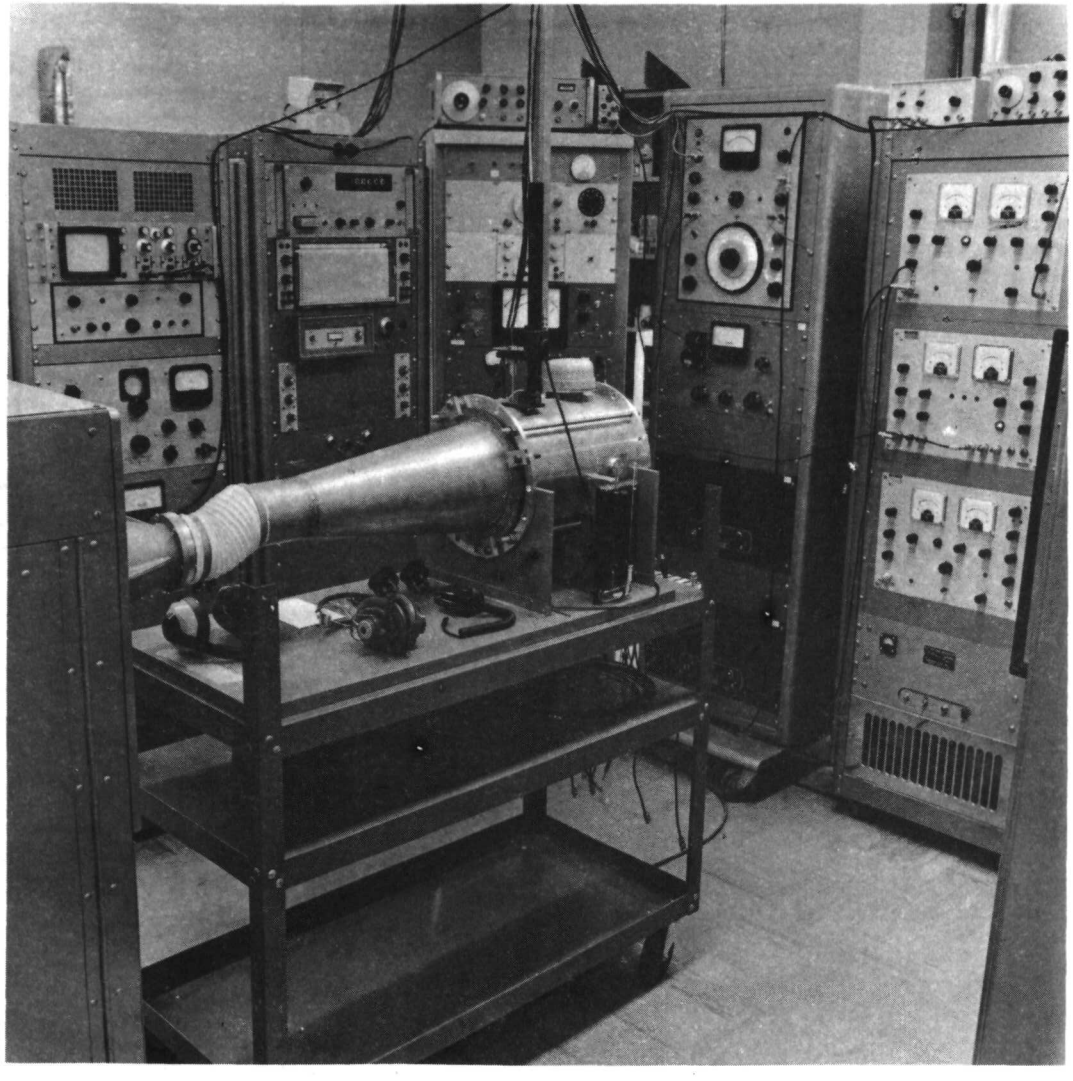

Figure 12. Photograph of the Experimental System - View 1.

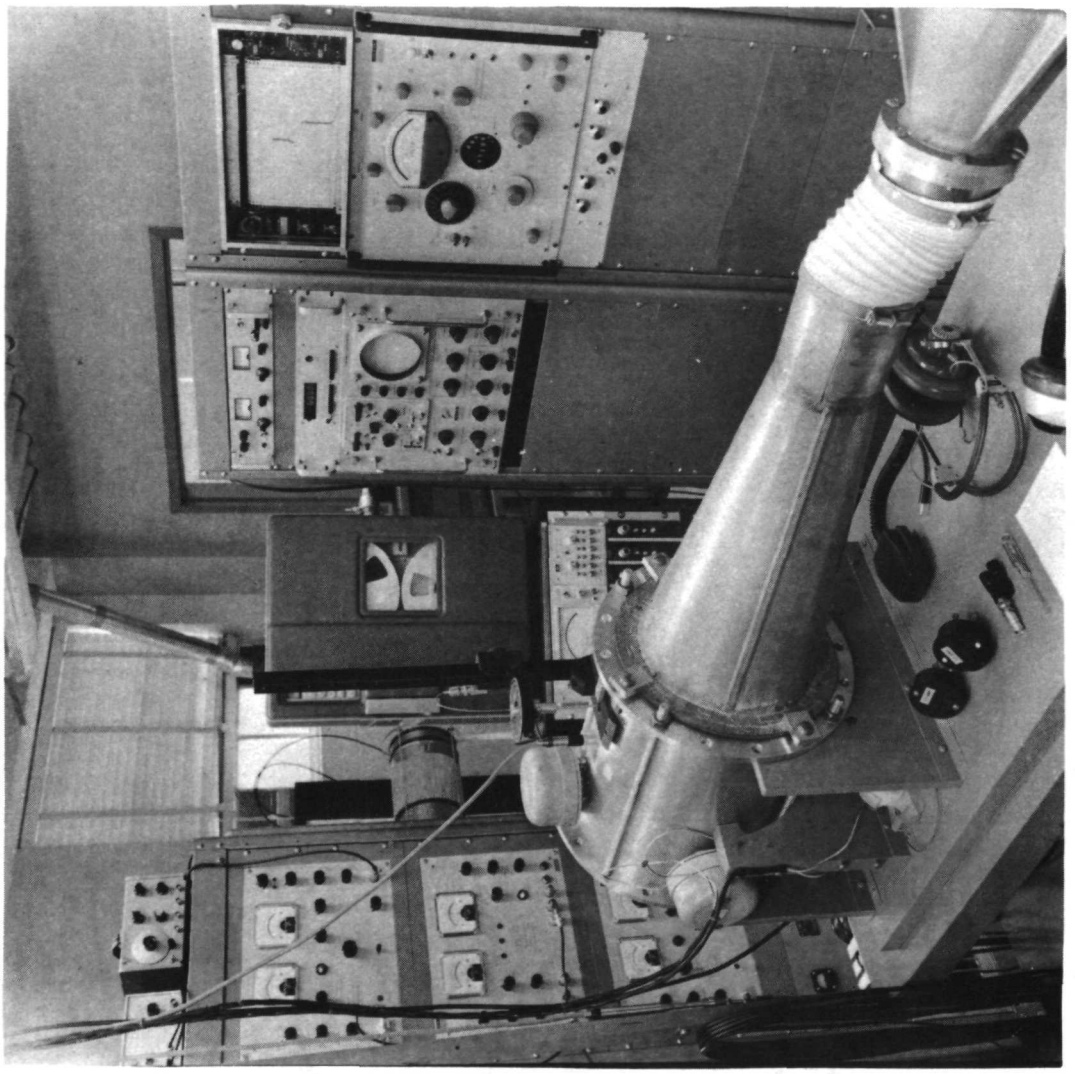

Figure 13. Photograph of the Experimental System - View 2.

drilled so that a flow of air can pass through the section. The cylinder and the endplates have an O-ring seal between them and the whole system is clamped together with four long bolts. The cylinder is divided into two sections, one 12.70 cm long, the other 17.78 cm long. They are joined with a lap joint containing an O-ring seal. The short section is for the acoustic drivers; the long section is for the hot wire and microphone probes. By dividing the cylinder into two parts, the drivers and probes can be positioned at any angle relative to each other.

The shorter cylindrical section has three threaded holes located at 0°, 90°, and 180° around the circumference, 6.35 cm from either end. Acoustic drivers can be mounted in any or all of these holes and plugs are available to close the holes when not in use. How many drivers are used, and which holes they are mounted in, depends on the type of sound field desired.

On the longer cylindrical section, provision is made for mounting two probe holding positioners, one which is adapted to hold a 1.27 cm condenser microphone with a probe tube extension, and one which can hold the hot wire probe support. Both have micrometer type scales which can position a probe to within 0.25 mm. The microphone holder is located so that the microphone probe moves along a diameter at the center of the test section. This enables a radial pressure profile to be measured. When it is only necessary to know the pressure at the wall of the chamber, the microphone positioner can be removed and a bare 1.27 cm microphone can be flush mounted in the wall of the chamber. Using a microphone without a probe tube extension eliminates the complex, frequency dependent calibration curve associated with it.

The hot-wire positioner is designed to hold Disa miniature hot wire probe holders. Its center is located 7 cm from the center of the test section so that when a right-angle probe holder is being used, the hot wire is located at the center of the test section and can be moved along the same radial line as the microphone probe. The right-angle probe is relatively short and can only penatrate a distance of 6.25 cm into the test section. To obtain velocity readings across the entire diameter of the section, a long straight probe holder can be used. However, for this case the hot wire will not be moving along a diameter at the center of the section. Figure 14 is a photograph of the test section with a right-angle hot wire probe holder in the system and a bare 1.27 cm condenser microphone flush mounted in the wall.

To generate a flow of air through the test section, it is connected via a sheet metal cone and flexible tubing to a fan which draws air through the system. The cone, flexible tubing, and fan housing can be seen in figures 12 and 13. To keep from drawing dust into the system, which might alter the characteristics of the hot-wire, or destroy it, an air filter was mounted at the inlet to the test section. This had to be eliminated, however, since access to the inlet had to be maintained in order to check the sound field being generated.

Sound Generation System

The distorted acoustic oscillations, which are required, consist of a spinning tangential cosine wave at the fundamental frequency with a cosine wave at twice this frequency added to it. The intensity of this sound should be about 160 dB or greater so that the acoustic pressures and velocities are significant compared to the background noise in the system.

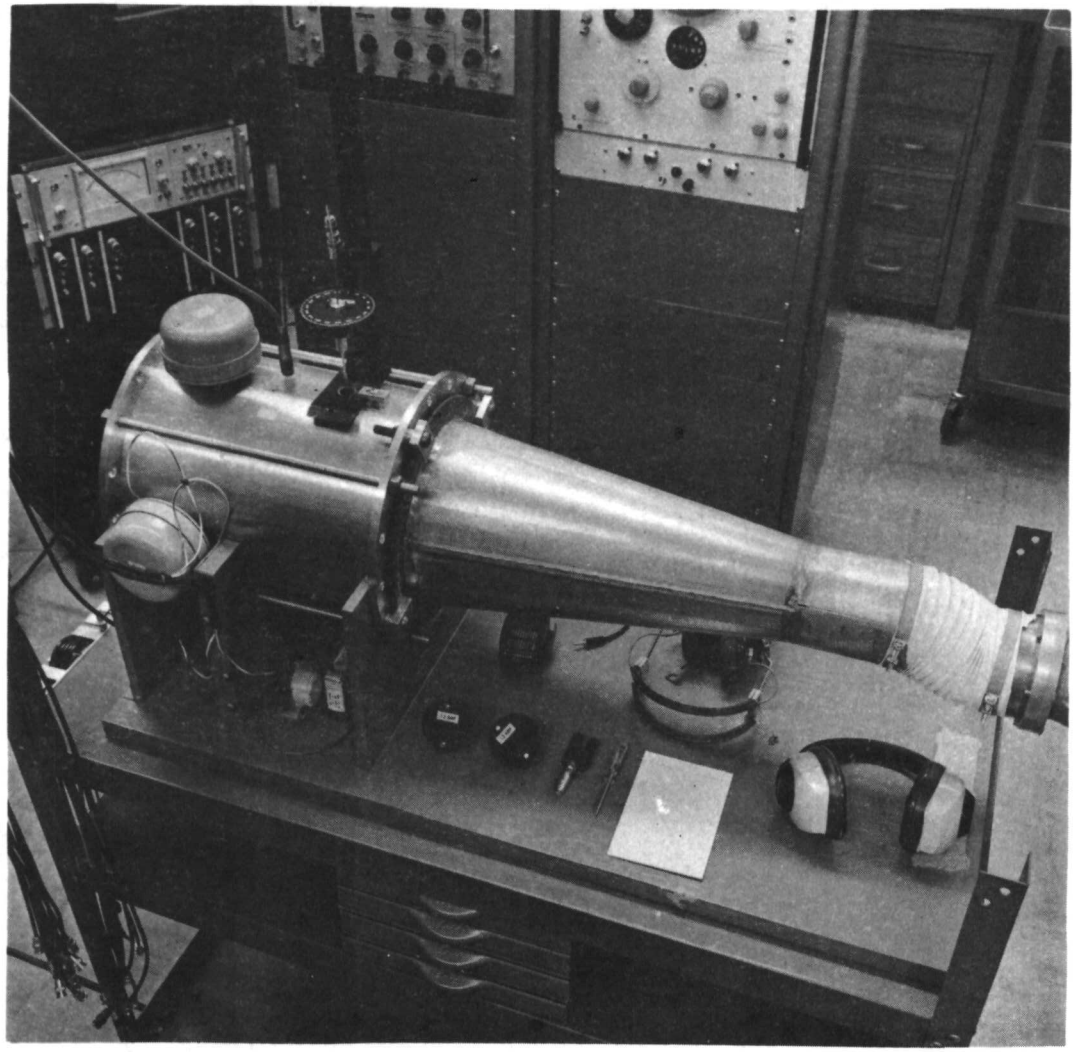

Figure 14. Test Section with Right-Angle Hot Wire Probe and Bare Microphone.

Theoretically, to create a spinning mode, two drivers are required, located 90° apart, which generate signals of the same amplitude and frequency, but 90° out of phase with each other. In actual practice, the signals going to the drivers may have to have slightly different amplitudes, and have a phase difference other than 90°, to produce a spinning mode. This is because the response of the drivers may not be exactly the same and the chamber itself interacts with the drivers. Thus, to generate the type of acoustic oscillations desired, two signals will have to be created containing the fundamental and the second harmonic frequencies, but whose amplitudes, both fundamental and second harmonic, can be adjusted independently, and whose phase differences can be adjusted relative to each other. Then, to create the desired sound field, adjustments to the phases and amplitudes can be made while monitoring the resulting sound field with an auxiliary microphone. The system used was outlined in Figure 11 and is shown in more detail in Figure 15. A cosine wave generated by the General Radio 1209-A function generator and tuned to the fundamental frequency is used as the basis of the sound generation system, with all other equipment adjusted relative to it.

The acoustic drivers are rated at 75 watts, but experience has shown that they cannot be used at this level when being driven by a pure tone, or a pure tone with one of its harmonics, without overheating. Because of this, they should not be driven to power levels above about 50 watts each. However, this is sufficient to generate sound levels of over 160 dB. When less complex acoustic oscillations are desired, parts of the system are simply not used.

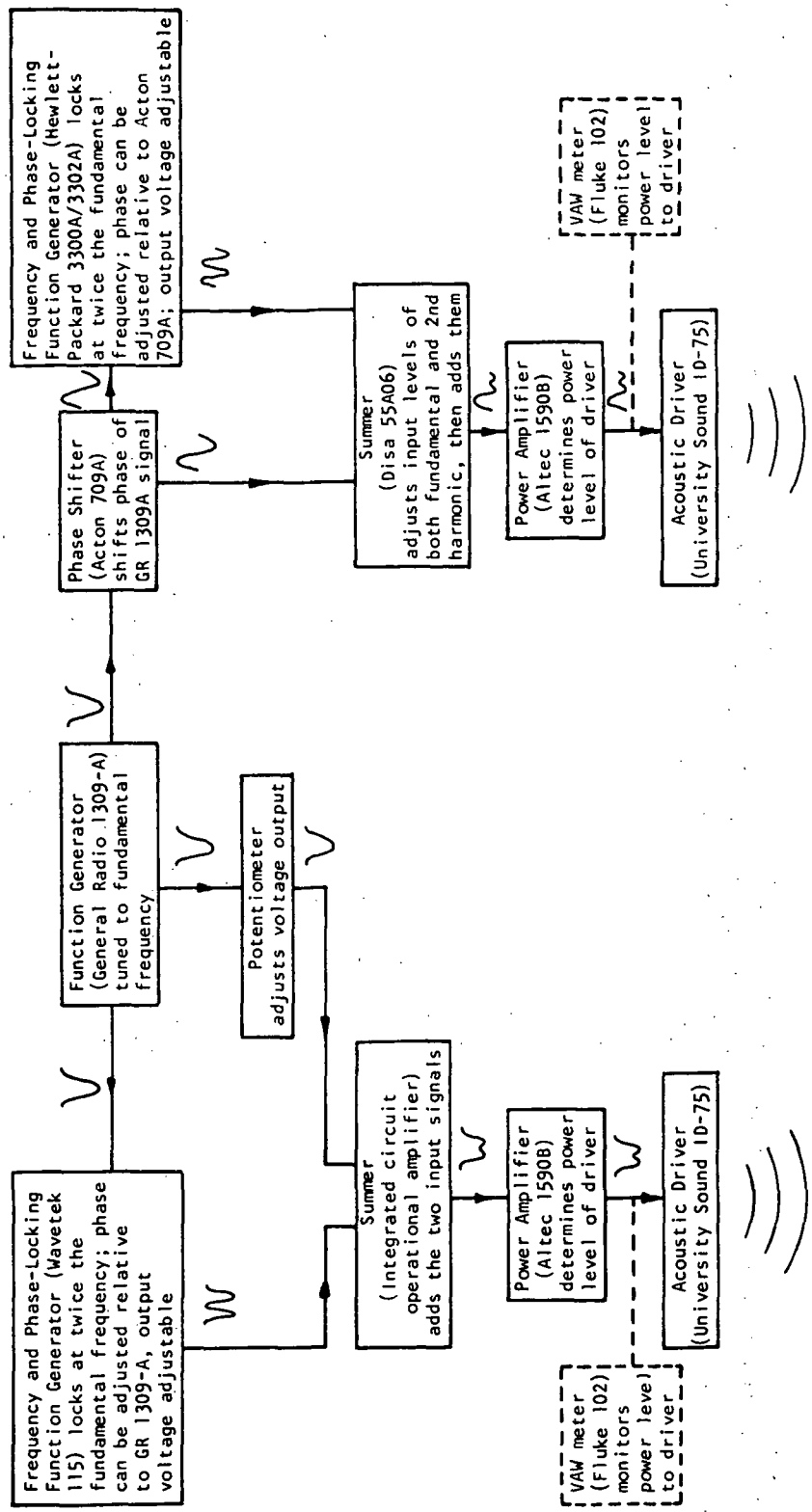

Figure 15. Sound Generation System.

Data Analysis System

The signals from the hot-wire and microphone must be processed to obtain a crosscorrelogram from which a response factor can be obtained. The system used was outlined in figure 11 and is shown in more detail in figure 16.

The signal from the hot-wire is processed by the constant temperature anemometer. The output of the anemometer is the sum of two components -- one caused by the through flow through the test section, the other a result of the acoustic velocity. An oscilloscope is used to remove the time-mean component of the anemometer signal. A sound level meter converts the output of the microphone to a signal proportional to the sound level. Both the resulting signals, E' and P', are then recorded on tape so the data is permanently recorded and can be analyzed from different aspects at later times. Also, recording the signals is in part made necessary by the intensity of the sound created by the system while in operation. It cannot be tolerated for long periods of time; hence, it is better to record the data, turn off the system, and then analyze the data.

Phase shifts and/or time delays may occur in the signals during processing. Because of this it is necessary to incorporate a time delay unit into the system to compensate for them. The time delay unit is controlled by the level of the DC voltage input to it. Two inputs are available to the system. One, a DC power supply, can be adjusted manually to the particular voltage and, hence, time delay, that is desired. The other is a function generator which inputs a continuously varying DC signal which can be adjusted to scan the entire range of time delays from zero to a complete fundamental period.

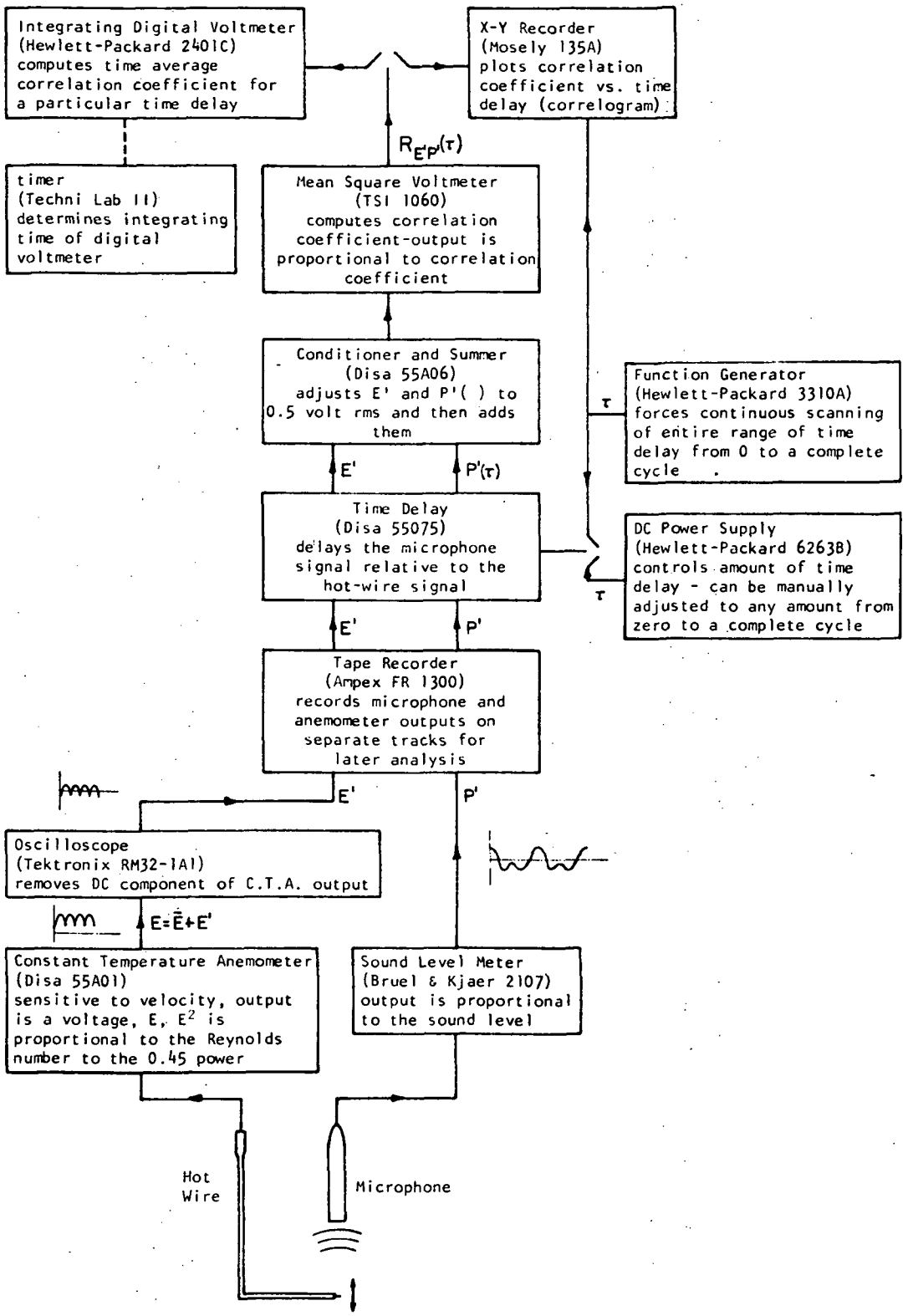

Figure 16. Data Analysis System.

After the signals have been delayed with respect to each other, they are each adjusted to 0.5 volts rms and added. A correlation coefficient is then calculated from this sum. This correlation coefficient can be processed in two ways. If the time delay is a constant (DC power supply controlling the time delay), an integrating digital voltmeter and a timer can be used to obtain a time averaged correlation coefficient for that particular time delay; or, if the time delay is being continuously changed, the correlation coefficient can be plotted against this time delay on an x-y recorder to obtain a crosscorrelogram of the data.

Auxiliary Monitoring Equipment

To operate the system properly, and to be able to analyze the data, various auxiliary monitoring equipment is necessary. The only way to determine what type of sound field is being generated is to monitor it with a microphone. A second 1.27 cm condenser microphone with probe tube extension is part of the system. The probe tube extension is 1 mm in diameter and thus can be inserted into the system through the holes in the endplates. In this way the sound pressure level can be checked at various angular positions at a constant radial distance from the center; or, the pressure variation along a diameter can be checked.

A phase angle meter is used for checking the phase between various signals. A dual trace oscilloscope is available to view the shapes of the various signals and especially to monitor the wave forms generated by the microphone and anemometer during data taking. To determine the frequency of the fundamental and its second harmonic, a frequency meter is available. These frequencies are not necessarily constant since they vary with temperature. Also, parts of the system

are various DC and AC voltmeters, wet and dry bulb thermometers, and a barometer.

Procedures

Before data is taken, all the equipment is adjusted and calibrated. Then the through flow and acoustic field are generated and data is recorded from the anemometer and microphone outputs. With the sound off, a crosscorrelogram is then made from the data. From this, response factors can be calculated. Different types of acoustic fields were generated in order to better understand the system itself and to help in analyzing the data for the spinning transverse mode.

Wire Calibration

To make a meaningful comparison between the analytical and experimental results, the equation relating air velocity to voltage output from the anemometer, which is used in the analysis, must be the equation that fits the particular wire being used in the experiment. To determine this equation, the wire has to be calibrated. The equipment used for this purpose is shown in figure 17 and consists of a very low turbulence wind tunnel and a micromanometer. These are used in conjunction with the hot wire anemometer to obtain the calibration. The tunnel has provisions for the mounting of a wire, connections to attach the wire to the anemometer and taps for connection to the manometer. The velocity of air through the tunnel can be determined from the pressure drop indicated on the manometer. To calibrate the wire, an overheat ratio must first be decided on. This determines the operating temperature of the wire relative to the ambient temperature and its value is a

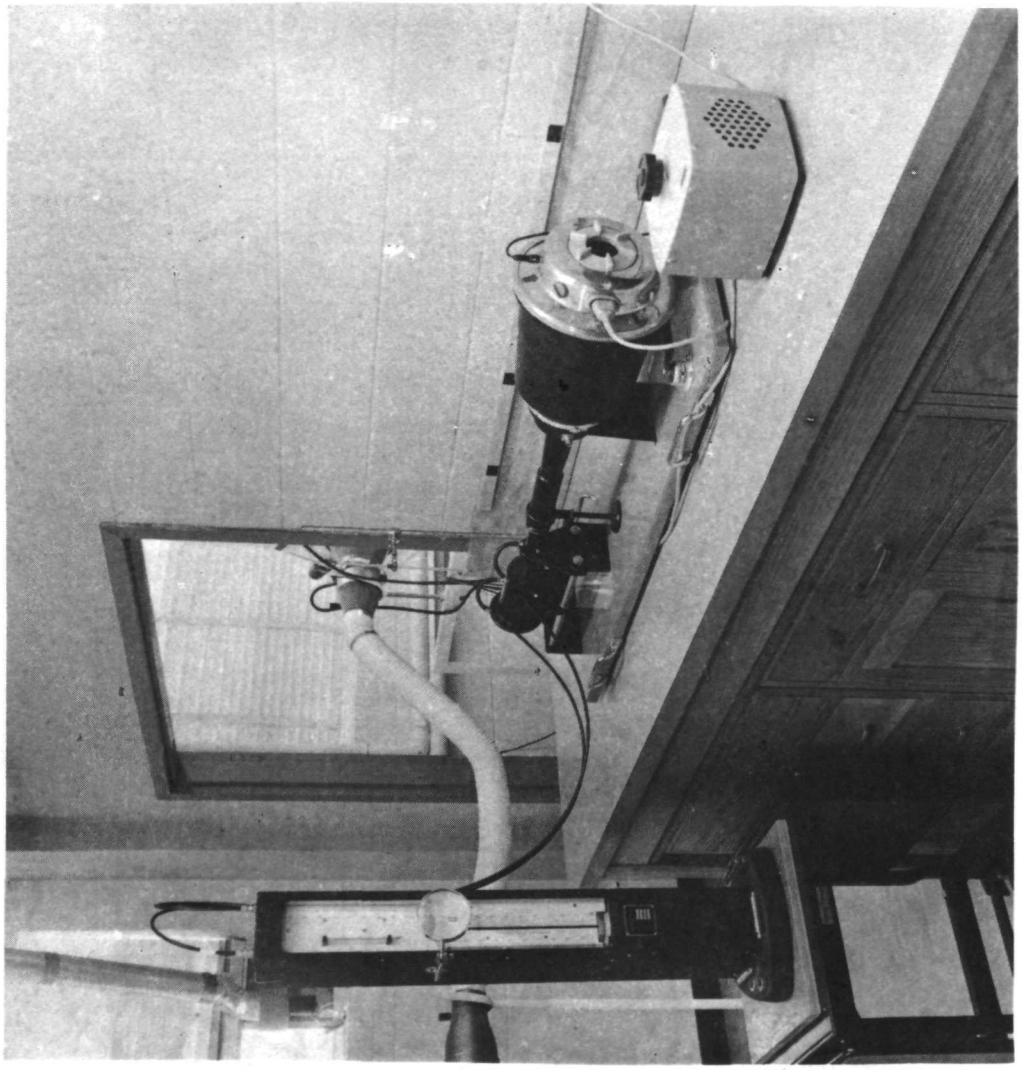

Figure 17. Hot Wire Calibration Equipment.

compromise between sensitivity and wire life. With higher operating temperatures more sensitivity is obtained, but there is a greater chance of contaminating or burning out the wire. So far, an overheat ratio of 1.4 has been used for all the experimental work.

After adjusting the anemometer to the desired overheat ratio, data are taken for the pressure drop on the wind tunnel and the voltage output from the anemometer -- in the range of velocities of interest. These data are then converted to velocity and voltage data, which in turn are used to determine the constants in the Collis-Williams equation. This last step is done by a least-squares curve fit of the data to the equation, using a computer. Figure 18 gives the data, computer plot and resulting equation for the calibration of a wire.

System Operation

In order to take data, a through flow of air is first established in the test section, The velocity of this flow is adjusted to a level where the velocity is significant compared to the turbulent fluctuations, which is at a level of about 2 m/sec. In later work this velocity may be changed to establish its effect on the response.

Next, the desired acoustic field is generated. This is done by installing the necessary acoustic drivers, tuning the General Radio 1309-A function generator to a cosine wave at the resonant frequency and feeding this signal via a power amplifier to one driver, and, if two drivers are being used, adjusting the phase shifter to the angle required at the second driver. Then the power to the drivers is increased to a value in the vicinity of that necessary to generate acoustic pressures and velocities which are significant compared to the background noise.

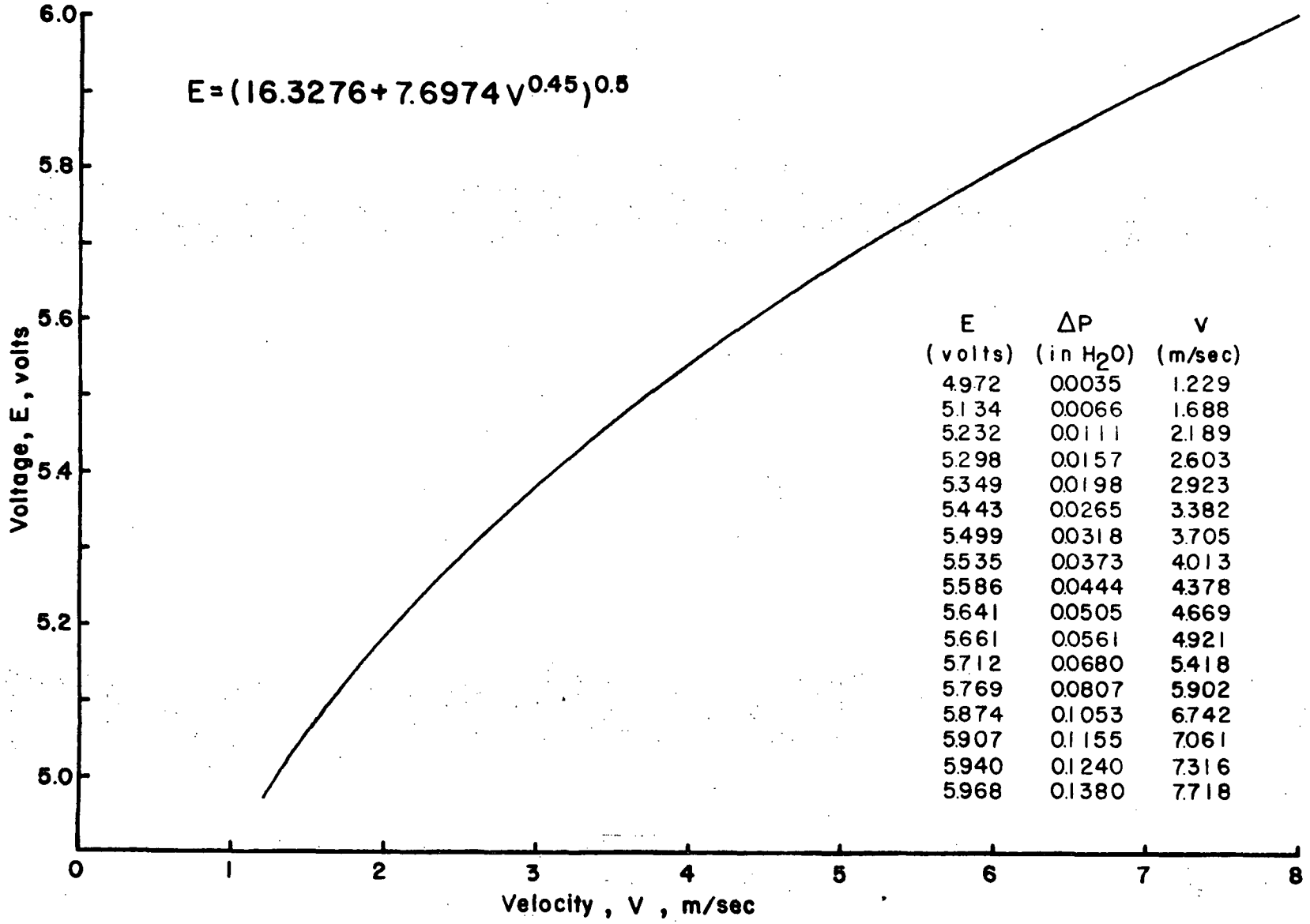

E (volts)	ΔP (in H_2O)	V (m/sec)
4.972	0.0035	1.229
5.134	0.0066	1.688
5.232	0.0111	2.189
5.298	0.0157	2.603
5.349	0.0198	2.923
5.443	0.0265	3.382
5.499	0.0318	3.705
5.535	0.0373	4.013
5.586	0.0444	4.378
5.641	0.0505	4.669
5.661	0.0561	4.921
5.712	0.0680	5.418
5.769	0.0807	5.902
5.874	0.1053	6.742
5.907	0.1155	7.061
5.940	0.1240	7.316
5.968	0.1380	7.718

Figure 18. Hot Wire Calibration Curve.

and through flow velocity. This is at a sound pressure level of about 160 dB. The phase shifter and the power to the drivers are then adjusted until the acoustic field has the proper characteristics. After that the desired distortion can be added by means of the Waveteck and Hewlett-Packard function generators.

The proper characteristics of the acoustic field depend on the type field being studied. For example, to obtain a spinning transverse field with distortion, a spinning field without distortion is established first. The characteristics used to determine if the spinning transverse mode is present are as follows:

- The amplitude of the sound is measured at numerous angular positions around the test section at a constant radial distance from the center. If the acoustic field is spinning, this amplitude should be constant.

- The change in phase as the microphone probe is moved around the circle is also checked. If the acoustic field is spinning, the phase change should correspond to the amount of change in the angular position of the measurement.

- The variation in the acoustic pressure along a diameter is measured. If it is spinning, $(P'/P'_{max})_{rms}$ should vary from one at the wall to near zero at the center with the decrease varying as a zero order Bessel function. Figure 19 compares such pressure data to the predicted Bessel function.

- The change in phase along a diameter is measured. It should be constant from the wall to the vicinity of the center. In crossing the center, the phase should change by 180° and then be constant again to opposite wall. Figure 20 is a plot of the phase angle along a diameter for various radial positions.

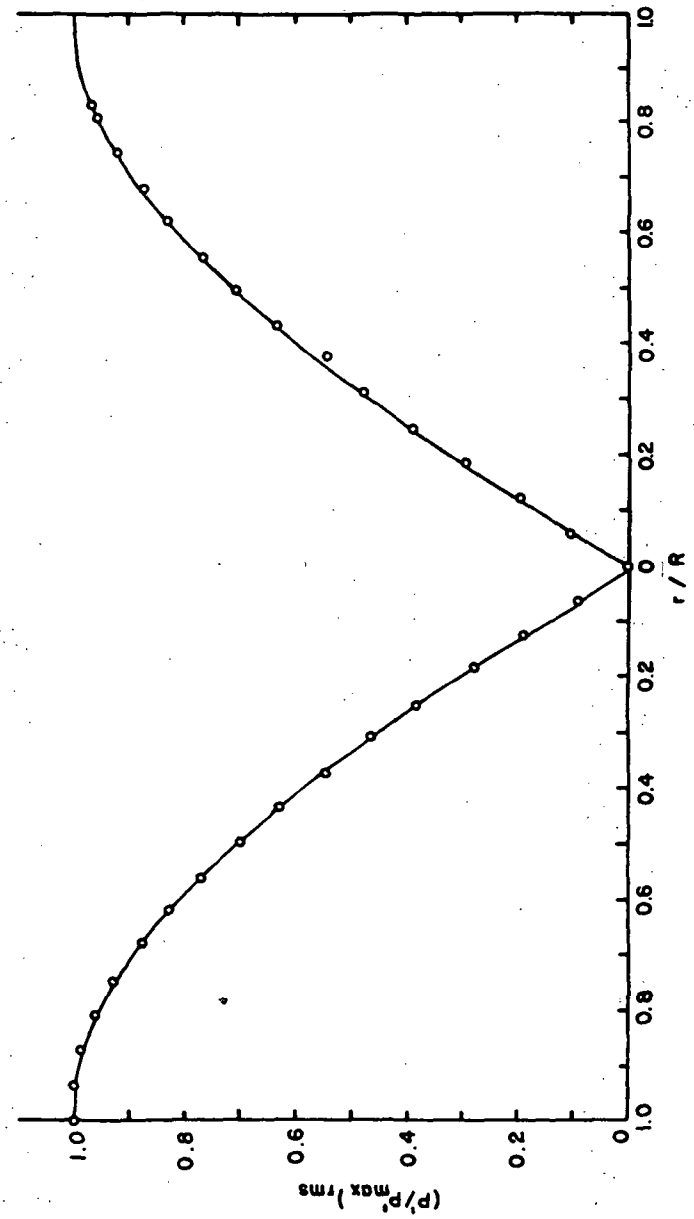

Figure 19. Sound Pressure Variation Along a Diameter.

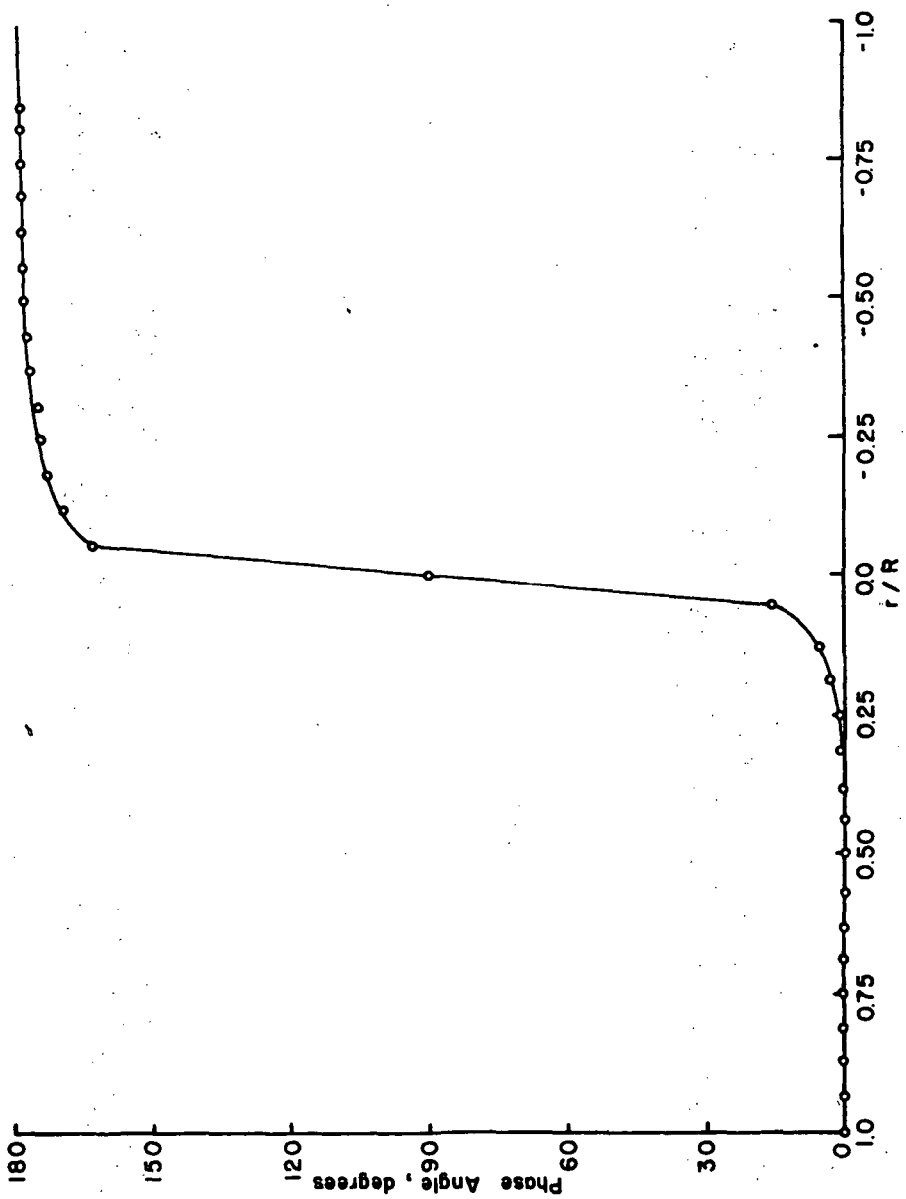

Figure 20. Change in Phase Along a Diameter.

After the spinning transverse mode is established, the distortion is added by first locking the Wavetek and Hewlett-Packard function generators to twice the fundamental frequency, then gradually increasing their amplitudes and adjusting their phases relative to the fundamental signals until the desired pattern of distortion is achieved. This is checked by monitoring the anemometer and microphone signals on an oscilloscope.

The theory correlates velocity and pressure at the same location, but experimentally both probes cannot occupy the same location. However, since the pressure varies in a predictable manner, as is illustrated in figure 19, if the pressure at any location (except the center) is known, the pressure at any other point can be computed. Thus if the position of the hot wire is measured relative to the microphone and chamber, the microphone data can be modified to indicate the value of the pressure at the hot wire rather than the pressure at its actual location.

The output of the anemometer goes to the Tektronix oscilloscope in order to remove $\bar{E}$ from the signal and to adjust the scale of the resulting signal so that it is within the 1-volt-rms limit on the input to the tape recorder. Also, the scale and range of the sound level meter are set so that the microphone signal is within the 1-volt-rms limit of the recorder. When this has been done the two signals are recorded. A record is kept of the settings on all the instruments used, along with temperature and atmospheric pressure measurements, and calibration results. When this has been completed, the sound, microphone,

and anemometer can be turned off, and the analysis can be done using the taped data.

The analysis has been done in two ways, both of which have advantages. In the first method the time delay of the microphone signal is set manually at selected values and the corresponding correlation coefficients are all determined from the same section of the tape. This is accomplished by continually recycling the tape over the same section for each time delay. In this way a crosscorrelogram is obtained in which external effects are kept to a minimum. The room temperature, the barometric pressure, and the characteristics of the equipment are the same since the same data are analyzed over and over. However, this method is time consuming and tedious and results in data points rather than a continuous plot.

The second method automates the procedure. A ramp function with a period of 2,000 seconds is used to drive the time delay unit. The amplitude of the ramp is adjusted so that it varies the time delay from zero to a value representing a complete cycle. The x-y plotter is then used to continuously plot a correlation coefficient versus the time delay. The disadvantage of this method is that the correlation coefficient is being calculated at different sections on the tape and the data vary from one section to another.

Results

Data were recorded for several different types of sound field -- spinning with distortion, spinning without distortion, and standing transverse. Final results have not been obtained as yet, primarily due to delays in obtaining the proper amplifiers for the system. All data

taken with a spinning acoustic field contained distortions due to the irregularities in the sound field created by the temporary power amplifiers.

In an attempt to account for the time delays introduced by the equipment, data were taken for the first standing tangential mode using a sine wave at the fundamental frequency. Pressure data were taken at the pressure antinode and velocity data were taken at the center of the test section (the velocity antinode). In theory, these properties are related in a relatively simple manner. Figure 21 compares the theoretical and experimental results and indicates that there is either a 40° or a 220° shift in phase. The reason for the difference in amplitude of the two curves has not been accounted for. It may result from an error in the computations or may possibly be due to the method of dealing with $\bar{E}$ and E' experimentally.

The correlation coefficient which is calculated experimentally is

$$R = \frac{\overline{E' P'}}{E'_{rms} P'_{rms}} . \tag{38}$$

The in-phase response factor can be obtained from R as follows:

$$R_{n\ell} = \left[\frac{\overline{E' P'}}{\overline{(P')^2}}\right] \left[\frac{\bar{P}}{\bar{E}}\right]$$

$$= \left[\frac{\overline{E' P'}}{E'_{rms} P'_{rms}}\right] \left[\frac{E'_{rms}}{P'_{rms}}\right] \left[\frac{\bar{P}}{\bar{E}}\right]$$

$$= R \left[\frac{E'_{rms}}{P'_{rms}}\right] \left[\frac{\bar{P}}{\bar{E}}\right], \tag{39}$$

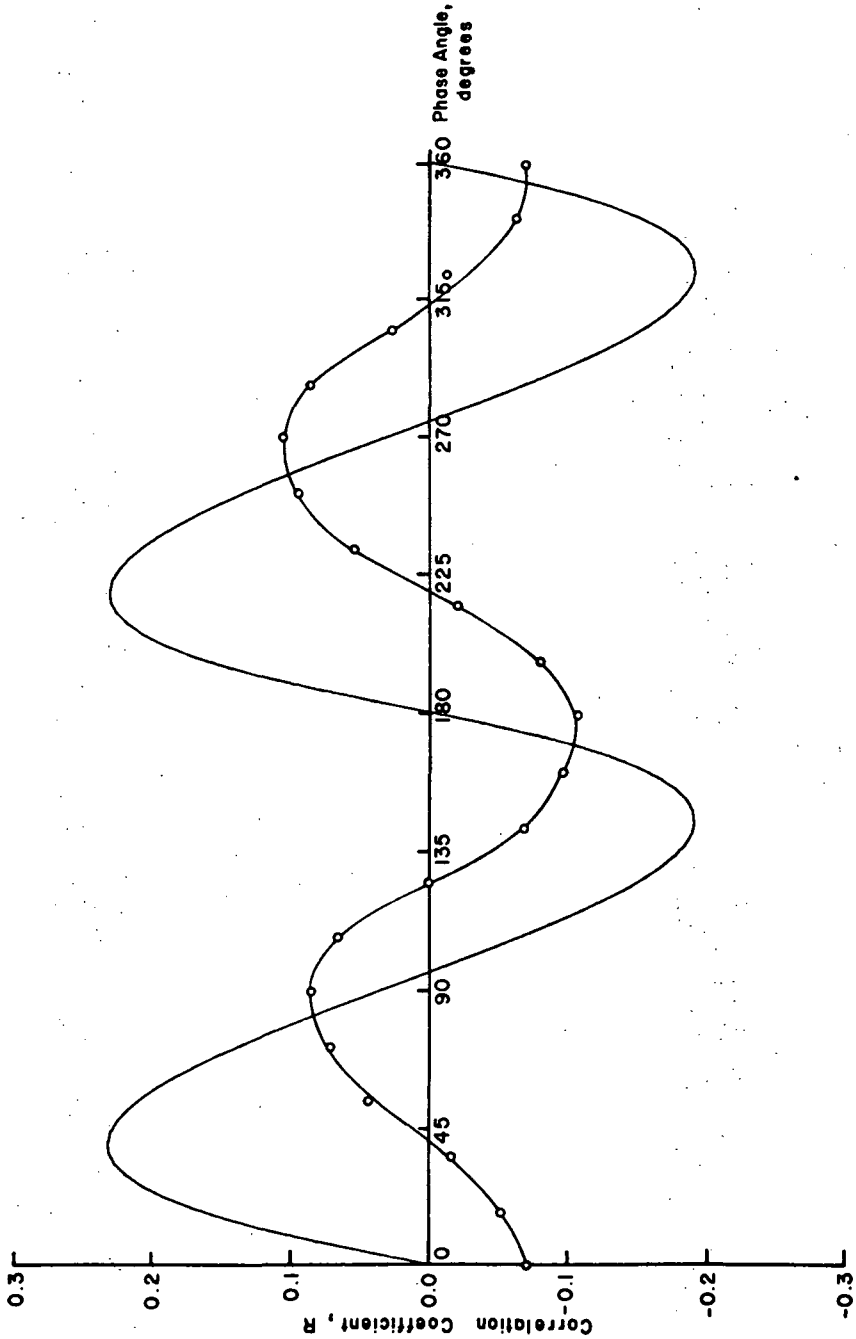

Figure 21. Experimental and Computer Crosscorrelograms for the First Standing Tangential Mode.

where $\bar{P}$ is the barometric pressure and $\bar{E}$ is the time-mean of the voltage from the anemometer.

Figures 22 and 23 show the experimental results obtained for the spinning transverse acoustic field with distortion as well as the analytically predicted results. As stated earlier, these results are not conclusive since they were obtained from sound fields distorted by the power amplifier.

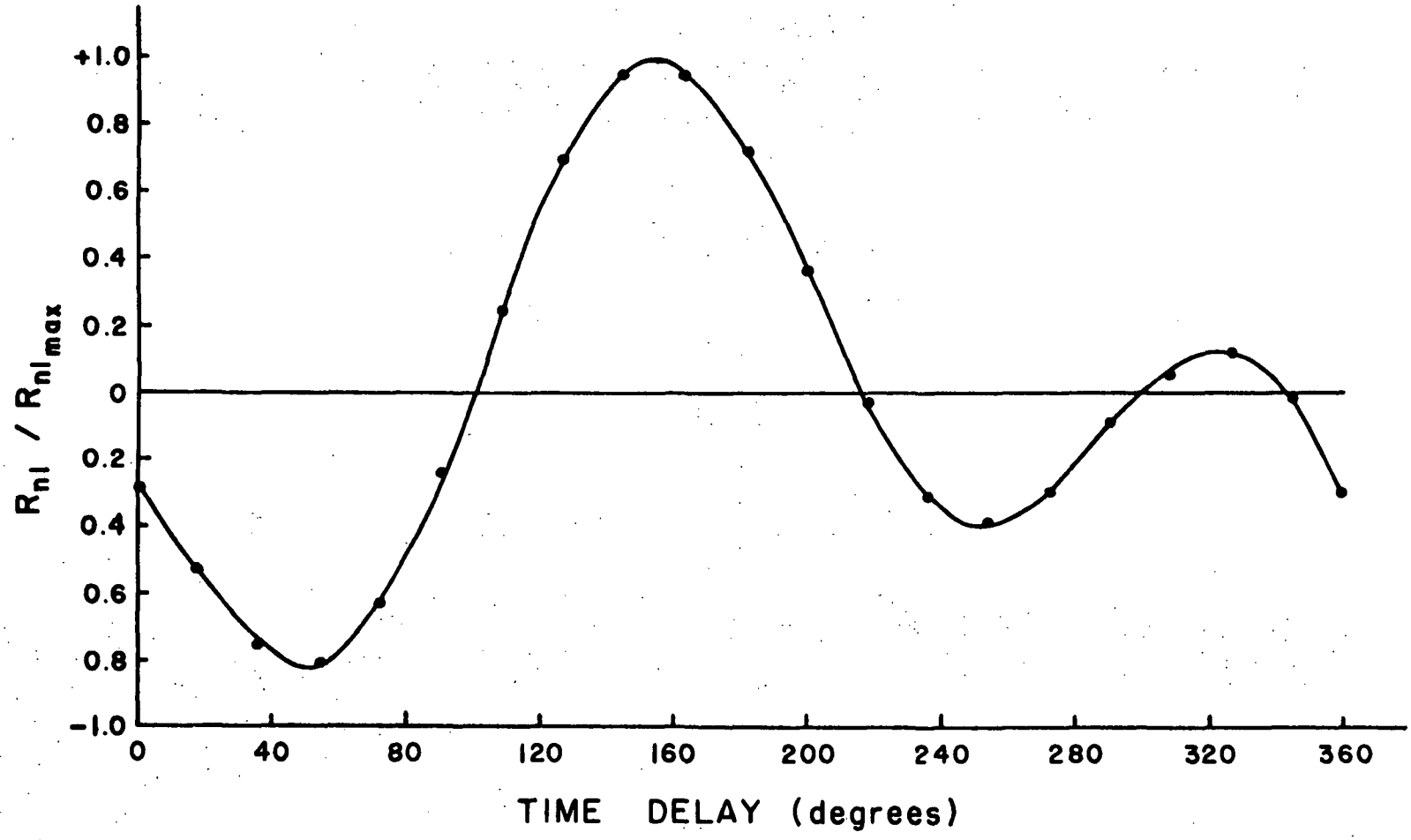

Figure 22. Experimental Time-Delayed Crosscorrelation Ratio.

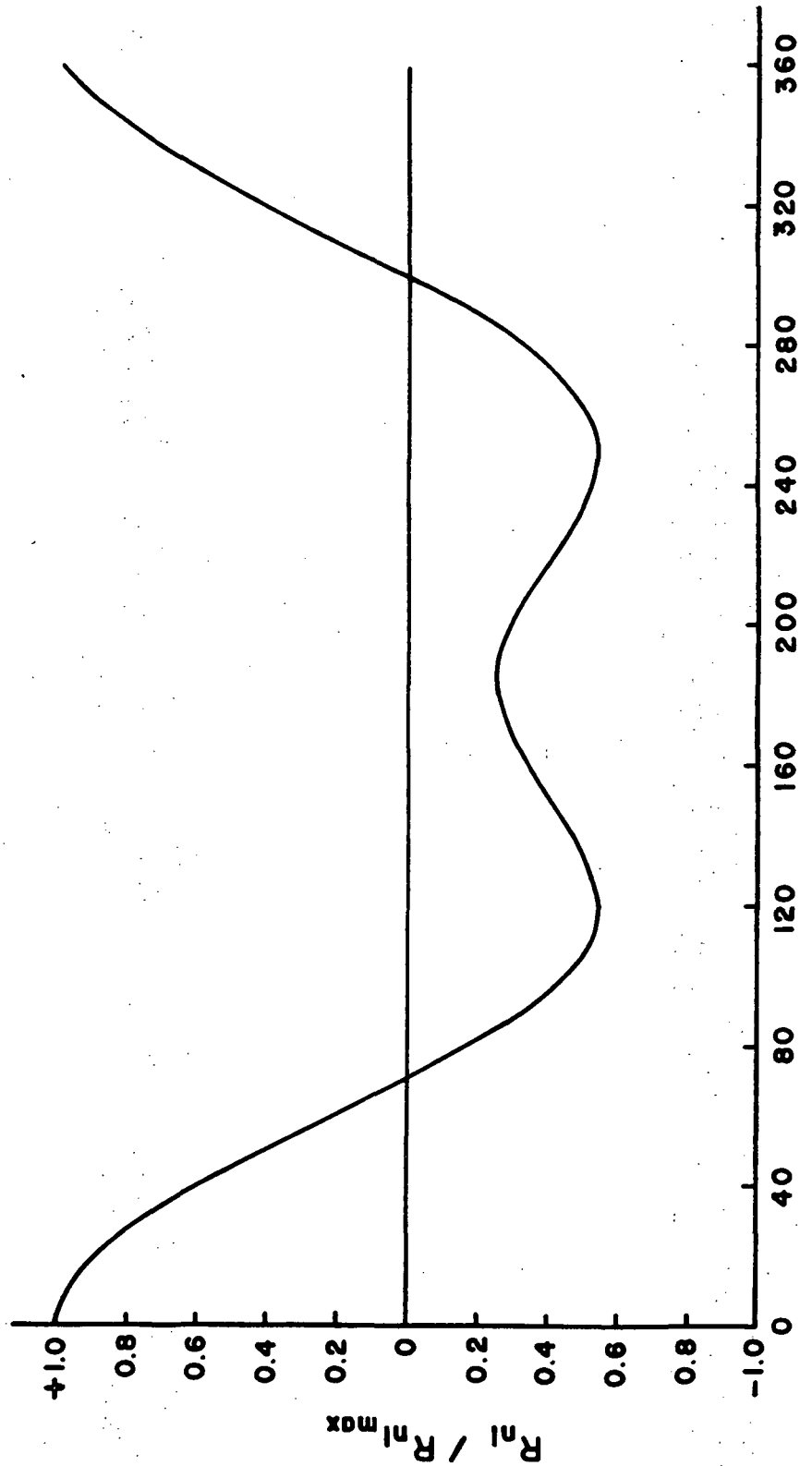

Figure 23. Predicted Time-Delayed Crosscorrelation Ratio for the Conditions of Figure 22.

Chapter 4

CONCLUDING REMARKS

The results obtained so far for both the analytical and experimental portions of the investigation indicate that the idea of using a hot wire as an analog of vaporization limited combustion is feasible. The desired acoustic vibrations can be created and a response factor obtained. However, the instrumentation required in the experimental portion has been found to be much more complex than originally envisioned. The system as a whole is still in need of precise calibration.

What has been done is only the preliminary work needed to create a working system. To obtain information useful to design, a feedback system must be set up so the system responds naturally rather than having a predetermined pattern of vibrations forced upon it. To realize the full potential of the system, a method of time delaying a complex signal will be necessary. Also, the system needs to be enclosed. The sound levels created during operation preclude use during normal working hours, and those operating the system can only tolerate the noise for short periods, even when using proper ear protection devices.

REFERENCES

1. Priem, R. J. and M. F. Heidmann: Propellant Vaporization as a Design Criterion for Rocket Engine Combustion Chambers, NASA TR R-67, 1960.

2. Heidmann, M. F.: Amplification by Wave Distortion in Unstable Combustors, AIAA Journal, vol. 9, no. 2, Feb. 1971, p. 336.

3. Heidmann, M. F.: Amplification by Wave Distortion of the Dynamic Response of Vaporization Limited Combustion, NASA TN D-6287, May, 1971.

4. Collis, D. C. and M. J. Williams: Two Dimensional Convection from Heated Wires at Low Reynolds Numbers, J. Of Heat Transfer, vol. 6, 1969, pp. 357-384.

5. Hilsenrath, J., et al., Tables of Thermal Properties of Gases, National Bureau of Standards Circular 564, November, 1955.